



## 26 **1. Introduction**

27 Rainfall volumes at varying duration and frequencies are required for the design of water management systems and  
28 facilities, like dams or dikes, spillways, flood retention basins, urban drainage systems, etc. These design precipitation  
29 volumes are also known as IDF (Intensity-Duration-Frequency) or DDF (Depth-Duration-Frequency) curves, and are  
30 derived from an extreme value analysis (EVA) on observed rainfall. For sampling extreme values, either annual maximum  
31 series (AMS) or peak-over-threshold (POT) can be used, however for return periods greater than 10 years, there are hardly  
32 any differences between the two. Often the AMS are preferred over the POT because the methodology is more direct and  
33 easier, whereas the POT method needs a prior assumption on the threshold selection. Afterwards a theoretical probability  
34 distribution (PDF) is fitted to the extreme series of a certain duration, in order to extract design rainfall volumes at specific  
35 frequency (or return periods). Typically, a Generalized Extreme Value (GEV) distribution is fitted for the AMS series  
36 and a Generalised Pareto for the POT series extracted for a fixed duration level. Rainfall extremes of different durations  
37 are strongly related to each other, however if the parameter fitting is done independently to each duration level these  
38 relations may not be kept (Cannon, 2018). Therefore, generalised concepts as in (Koutsoyiannis et al., 1998), simple  
39 scaling (Gupta and Waymire, 1990) or multi scaling Van de Vyver (2015) approaches are used to smooth the extreme  
40 statistics over different duration levels. Finally, since the rainfall observations are mostly point measurements, a  
41 regionalisation procedure of the PDF parameters to un-observed locations is performed. Methodologically, a distinction  
42 can be made between two approaches: a) a direct regionalisation of quantiles, moments or parameters of distribution  
43 functions and b) a regional estimation of distribution functions for homogeneous regions. Borga et al. (2005) suggests the  
44 regionalisation of the parameters instead of the quantiles. For the direct regionalisation of parameters, regressions  
45 (Madsen et al., 2009; Smithers and Schulze, 2001), splines (Johnson and Sharma, 2017) or kriging methods (Ceresetti et  
46 al., 2012; Kebaili Bargaoui and Chebbi, 2009; Uboldi et al., 2014; Watkins et al., 2005) are applied. On the other hand,  
47 the estimation of regional distributions functions based on the index method proposed by Hosking and Wallis (1997), is  
48 one of the most used methods in the literature for the regionalisation of design precipitation (Burn, 2014; Durrans and  
49 Kirby, 2004; Forestieri et al., 2018; De Salas and Fernández, 2007).

50 Since the analysis is performed on extreme values, first very long observations are required to ensure a proper fitting of  
51 the GEV parameters, particularly of the shape parameter which is of decisive importance for extremes of high return  
52 period (larger than 20 years return period). For instance, Koutsoyiannis (2004a,b) showed clearly that short time series  
53 (less than 50 years) can choose falsely a shape parameter of zero (Gumbel distribution) and hide the true heavy-tail  
54 behaviour of rainfall extremes (also supported by Papalexiou and Koutsoyiannis (2013) and Papalexiou (2018)). Second,  
55 a dense observation network should be available to ensure an adequate estimation of extreme value statistics also at un-  
56 observed locations. A less denser network would cause for instance that the kriging interpolated values to be less accurate  
57 and the spatial features to be more smoothen in space (Berndt et al., 2014). On the other side, index-based regionalisation  
58 can provide more robust estimation at un-observed locations if larger samples (obtained from denser networks) are used  
59 (Requena et al., 2019). Third, a high-resolution observation network (with 1- or 5- time steps) is as well necessary to  
60 estimate extremes of short durations (at scales of minutes or hours) for catchments that respond quickly to rainfall events  
61 (i.e., urban or mountainous areas prone to flash floods). At the moment, no perfect observation network that fulfils these  
62 three criteria is available, however different networks or datatypes fulfilling two criteria co-exist. For example, daily  
63 observation networks are typically very dense (every 10km) and can have up to 100-150 years of observations, but don't  
64 capture the extremes at sub-hourly durations. Digital tipping bucket or weighting sensors can measure the rainfall at 1min  
65 time steps and can be dense (every 20-25km), however they are available mostly after 2000 and hence too short for EVA.  
66 Long observations at 1min time steps from analogous Hellmann or tipping buckets may be available from 1900-1950  
67 only at some countries (i.e. Germany, Belgium) but are not as dense as digital or daily measurements (>50km).

68 Alternatively, weather radar or satellite data can provide rainfall fields at 1- or 4-km<sup>2</sup> and 5min time steps, but offer short  
69 observations (less than 20 years) and suffer from high inaccuracies (Marra et al., 2019).

70 To optimize the DDF estimation, different data types have been combined for instance; Madsen et al., (2017) regionalised  
71 extremes in Denmark from 1min observation with daily interpolated values as a co-variate, Bara et al. (2009) employed  
72 the simple scale principle to derive DDF curves for sub-daily duration levels (5min – 3h) from daily observations in  
73 Slovakia, Goudenhoofdt et al., (2017) used station observations (10min and varying lengths) to correct radar data and  
74 estimate the hourly and daily extremes, Burn (2014) pooled together long and short observations at 5min time steps to  
75 form the DDF curves in Canada. However, care should be taken when combining information from data types that differ  
76 in observation length, temporal and spatial scales. Holešovský et al. (2016) separated the historical data into groups when  
77 estimating DDF curves for Czech Republic (long series with 35-40 and short series with 11-15 years of observations) and  
78 concluded that the uncertainty at estimating parameters for the short time series is quite high, especially for high return  
79 periods. In the index-based regionalisation, regional L-moments are averaged based on the observation length, which may  
80 lead to more stable results (Burn, 2014; Requena et al., 2019), however the interpolated index may still suffer from high  
81 uncertainties from pooling together short and long time series. This may also be the case when interpolating local GEV  
82 parameters with the kriging theory. The regionalisation of the shape parameter may be not representative if short and long  
83 observations are pooled together with same importance, thus keeping a fix shape parameter may help to mitigate this  
84 problem. Nevertheless, further investigation should be done to ensure if long observations, as more reliable, should have  
85 more importance than the short ones when regionalising extreme value statistics. Regarding the temporal scale difference,  
86 a study from Paixao et al. (2011) performed in Ontario Canada concluded that the scaling factors should not be used for  
87 downscaling daily extremes to durations less or equal to one hour. This is because the extremes at such short durations  
88 are governed by other rainfall mechanisms than the daily extremes, and hence a low dependency exists between the two  
89 extreme groups. Alternative to the scaling principle, disaggregation schemes can be applied to the daily data in order to  
90 obtain adequate extremes (with return period up to 5 years) for sub-hourly durations (Müller and Haberlandt, 2018). On  
91 the other hand, because of the spatial scale inconsistency between weather radar and gauge observations, the weather  
92 radar may not be appropriate to estimate directly extremes of short durations (Marra et al., 2019), however they can still  
93 be useful to extract sub-daily extremes if used to disaggregate daily observations as done by Bárdossy and Pegram (2017).

94 More complex disaggregation procedures that take advantage of the radar information by implementing an extensive  
95 parameter-set as suggested by Lisniak et al. (2013), may also be used to disaggregate daily observation and estimate the  
96 extreme values at sub-hourly durations. Nevertheless, to authors knowledge, there is no study in the literature that  
97 investigates if disaggregated daily time series can be useful in regionalising extreme values statistics when high resolution  
98 data are present, and when so, if they should have the same weights as high-resolution data.

99 Lastly, due to lack of data, in most of the literature, the combination of any two or alternative data types for EVA is  
100 validated on observations that are not dense or long enough (longer than 40-50 years). Therefore, it would be interesting  
101 to test different methods for estimation and regionalisation of DDF curves extracted from different datatypes, on a long  
102 and dense network. The German Weather Service (DWD) has a relatively dense observations network (every 50km) of  
103 1min rainfall data available from 1950 (60-70years), that enables a proper validation of EVA for return periods up to 100  
104 years. Additionally, denser digital observations (every 20km) at 1min time steps (mainly from 2000), very dense (every  
105 10km) daily observations (10-120years) and weather radar observations (from 2000) at 1km<sup>2</sup> and 5min time steps are as  
106 well available. As multiple data types co-exist in Germany, it is important to investigate the suitability of methods and  
107 data types for the extraction and regionalisation of extreme statistics while validating only at the long and dense  
108 observations. In Germany, studies either use the Koutsoyiannis approach or multi/simple scaling approach of GEV  
109 parameters to generalise the extremes over different durations. To authors knowledge there is no comparison of the two

110 approaches in the literature. The Koutsoyiannis approach has been implemented in Germany by Ulrich et al. (2020), but  
111 on a shorter available 1 min dataset (up to 14 years), while Fischer and Schumann (2018) have implemented the multi  
112 scale approach only at a long station (~85 years). Here we investigate which of these methods gives more accurate and  
113 precise estimation of DDF based on the long and 1min rainfall data. The same is true also for the regionalisation  
114 approaches: to authors knowledge there is no comparison between kriging and index-based regionalisation. Naturally, it  
115 is interesting to see which of the methods is more appropriate when validated on a long and high-resolution network, and  
116 where lie the advantages and disadvantages of each method when different data types are integrated, and what  
117 combination brings the best outcome. For this purpose, we investigate here three competitive regionalisation methods  
118 (ordinary kriging, external drift kriging and index-based regionalisation) based on different combination of data types  
119 (long series, short series, disaggregated daily series from weather radar parametrisation), while validating only on the  
120 long and high-resolution observations. At the moment, a revision of the current design storm maps in Germany  
121 (KOSTRA-DWD) is required in order to use additional data and state-of-the-art methodology. Therefore, an additional  
122 aim of this study, is to give the basis for development of the new design storm maps in Germany (KOSTRA-2023).

123 The paper is structured as follows: first the available data sets for extreme value analysis are introduced in Section 2, then  
124 the methods selected for investigation of the local and regional estimation are presented respectively in Section 3.1 and  
125 3.2, with performance assessment and validation explained in Section 3.3. The results are given for each objective as:  
126 best local estimation of extremes in Section 4.1, best regionalisation technique 4.2.1, best data integration 4.2.2. Finally,  
127 the obtained maps for Germany are discussed in section 4.3 and conclusions are given in Section 5.

## 128 **2. Study Area and Data**

### 129 **2.1 Available Data**

130 The study area covers Germany and is illustrated in **Figure 1**. Three rainfall measuring networks are available  
131 from the German Weather Service (DWD); the daily series (DS) – typically Hellman devices recording the rainfall daily,  
132 the long series (LS) – mostly tipping bucket analogue sensors (before 2004) measuring rainfall at 1 min time steps with  
133 0.1mm resolution and 2% uncertainty, and the most recent short series (SS) – digital sensors (after 2004) measuring  
134 rainfall also at 1min timesteps with 0.01mm resolution. The spatial distribution of these data series is shown in **Figure 1**,  
135 the observation length is given respectively in **Figure 2** and the number of stations available for each one is given in  
136 **Table 1**. The LS dataset is the most appropriate data set for extraction and evaluation of extreme rainfall statistics, since  
137 on average it includes 65 years of observations (as shown in **Figure 2**– dark blue) and measures the rainfall at very fine  
138 temporal scales. Nevertheless, this network is sparse in comparison to the other two, and only 133 stations in Germany  
139 are available. On the other side the SS dataset measures the rainfall as well at very fine temporal scales and is much denser  
140 than the long series (1261 stations excluding the LS locations), however on average it includes only 18 years of  
141 observations which is not enough for extreme value analysis. Lastly the DS dataset is much denser (with 4068 stations  
142 excluding LS and SS locations) and covers 40 years up to 120 years, but the temporal resolution of rainfall is too coarse  
143 to be useful for sub hourly extreme values analysis.

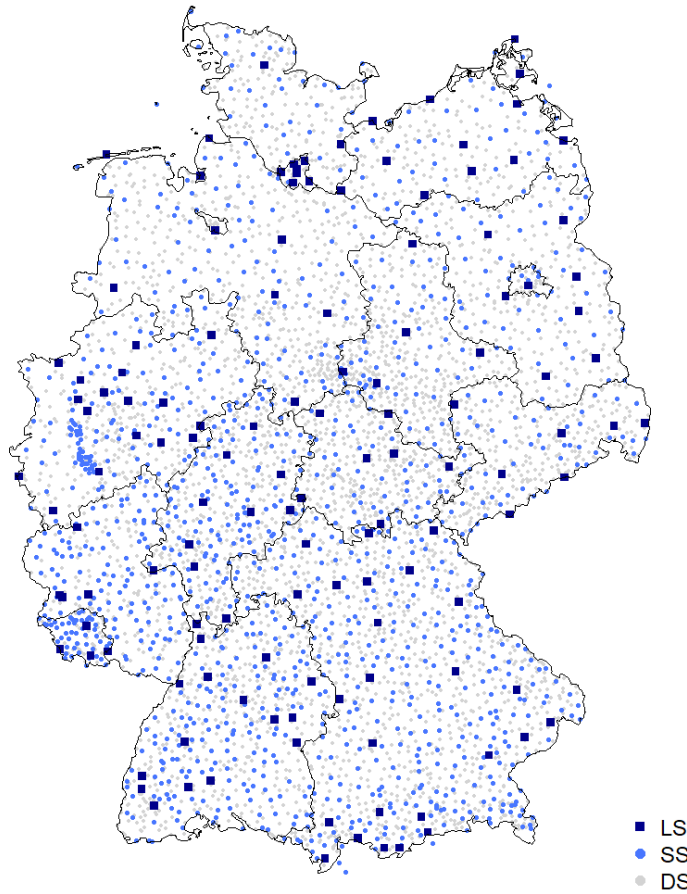


**Figure 1** Available rainfall data types in Germany categorized in three groups: long series (LS), short series (SS), and daily series (DS). The black lines illustrate the borders of German Federal States.

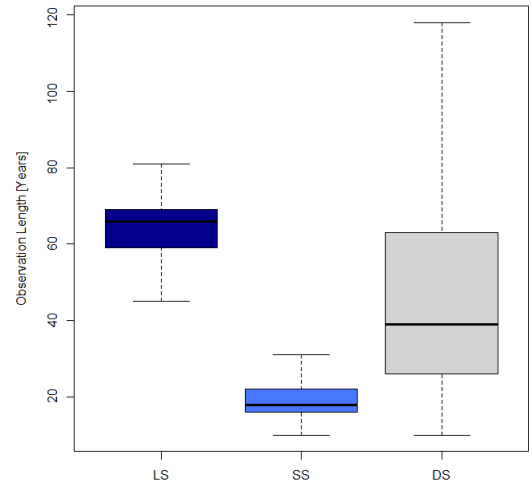


**Figure 2** Observation length of all stations grouped according to the three available data types in Germany: long series (LS), short series (SS), and daily series (DS).

**Table 1** Number of stations for each of the available data types in Germany: long series (LS), short series (SS), and daily series (DS)

Resolution	5min	1 day	
Obs. Length	> 41y	> 10 y	>10 y
No. Gauges	133	+1261	+4068

## 144 2.2 Temporal Disaggregation of the Daily Series

145 The daily dataset (DS) is much denser than both long and short ones and includes even longer observation periods than  
 146 the LS dataset. If it is possible to disaggregate these data reliably, this will considerably increase the number of support  
 147 points for the regionalisation of DDF curves. For the considerations presented here, the so-called cascade model first  
 148 introduced by Olsson (1998) is employed. A more extensive parameterisation is implemented in the method according to  
 149 Lisniak et al. (2013) which corresponds to a transfer of the Olsson method to a 3-fold distribution. To generate sub-hourly  
 150 data, disaggregation parameters are derived from the RADOLAN weather radar time series of each grid cell (Bartels et  
 151 al., 2004), and the daily observed volumes are disaggregated for the given durations as shown in **Table 2**. It is important  
 152 to note that, due to the parameterisation using RADOLAN data, no parameter regionalisation is required, so that the  
 153 parameter-rich disaggregation procedure in the Lisniak variant can be used. Moreover 30 realisations of disaggregated  
 154 data were generated for each duration, in order to capture the uncertainty due to the disaggregation. It was evaluated that  
 155 the relative error doesn't improve significantly for more than 30 realisations, as also reported in Müller and Haberlandt  
 156 (2018), therefore only 30 realisations of disaggregated data were used in this study.

**Table 2** The disaggregation scheme applied to the daily data (DS) to obtain rainfall volumes at the given durations.

Duration	12h	8h	6h	4h	3h	2h	1h	30min	15min
Disaggregation	24h / 2	24h / 3	24h/2 <sup>2</sup>	24h / 3/ 2	24h/2 <sup>3</sup>	24h / 3/ 2 <sup>2</sup>	24h/3/2 <sup>3</sup>	24h/ 3/2 <sup>4</sup>	24h/ 3/2 <sup>5</sup>

157 To understand what errors can be introduced to the DDF curves when employing this disaggregation scheme, a direct  
 158 comparison was conducted between the long series (LS) and the disaggregated daily series (DS) for the return periods 1,  
 159 10, 20, 50 and 100 years. For each station, duration level and return period, the relative error is calculated as the difference  
 160 between the disaggregated and the original rainfall quantile. The resulting deviations for all stations are shown in **Figure**  
 161 **3**. The results indicate that at the longer duration levels (>6 hours), the DDF curves are captured quite well, and the main  
 162 disadvantage of the disaggregation model (as expected) is for the very short duration. Below the duration of 4 hours, there  
 163 is a clear tendency to underestimate the extremes from LS, up to a median underestimation of 14% at the 30min duration  
 164 level. At the duration of 15min, a weakening of the underestimation is observed, which is probably due to the nonstationarity  
 165 in the original series identified in Section 2.4 below, which predominates only at duration levels up to 15min. Thus, it is  
 166 expected for the DS disaggregation scheme to be more useful for the longer duration extremes than the short ones,  
 167 particularly the extremes at sub-hourly durations.

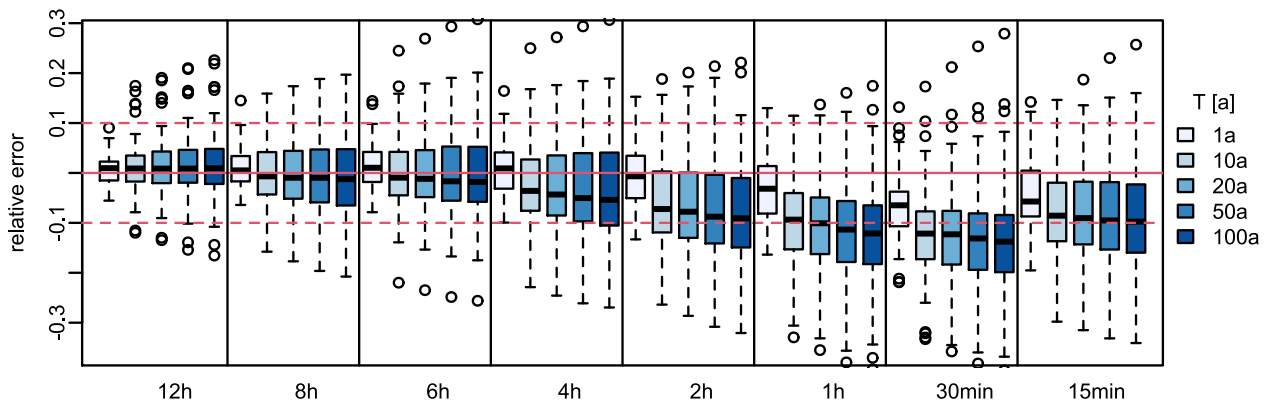


**Figure 3** The relative error (-) of the disaggregated daily station data (30 realisations) based on radar parametrisation for different return periods and duration levels: (+) sign indicates overestimation, while (-) sign underestimation of extremes. Different blue shades indicate the error at different return periods (in years) as shown in the legend (ex. 1a is one year return period).

### 168 2.3 Annual Maximum Series for Each Dataset

169 Using the five-minute time series, annual maximum series (AMS) are derived based on the calendar year for the duration  
 170 levels 5min, 10min, 15min, 30min, 1h, 2h, 6h, 12h, 1d, 2d, 3d and 7d. A moving window with the length of each duration  
 171 level is used to derive the annual maxima, considering a dry duration of 4 hours to ensure that the maxima selected in  
 172 December and January of two consecutive years are independent from one another. Additionally, following the guidelines  
 173 given by DWA (2012) a scaling of the durations 5, 10 and 15 min AMS with the factors given in **Table 3** is performed.  
 174 This is done to avoid the systematic underestimation of rainfall extremes at short duration caused by the deviation between  
 175 i) the start of the actually largest rainfall sum of duration D, and ii) the fixed starting time of the 5 min time series  
 176 (employed here).

**Table 3** Correction factors for Annual Maximum Series (AMS) of short duration according to the DWA-531 (DWA, 2012).

Duration level	5min	10min	15min
Correction factor for AMS	1,14	1,07	1,04

## 177 2.4 Homogenisation of Long and Short Dataset

178 First plausibility and homogeneity checks were performed on the long and short datasets, herein referred to as respectively  
179 long series (LS) and short series (SS). An initial analysis of possible trends based on the quantile regression (Koenker,  
180 2005) was carried out for the monthly 5min maximum intensities of the long series (LS). This method was chosen, as in  
181 comparison to the classical regression is considerably more robust and it allows to obtain regression results for different  
182 non-exceedance probabilities. In **Figure 4**, the quantiles for the non-exceedance probabilities  $\tau = 0.5$  (i.e. median), 0.8,  
183 0.9 and 0.95 are considered. Quantile regressions for the four selected  $\tau$  with time as the explanatory variable are  
184 implemented separately for each of the 133 measurement points. Each dashed line corresponds to a measuring station and  
185 each colour to a non-exceedance probability. Trend-like changes in the monthly five-minute maxima are visible with  
186 slopes that increase with  $\tau$ . To understand why this trend is present in almost all long series, we investigated whether  
187 these instationarities are more trend-like or jump-like, with the latter assuming that the timing of jumps is associated with  
188 sensor changes in the measuring network. In the long series, a total of 19 different sensor types are distinguished simply  
189 by two states: analogue or digital.

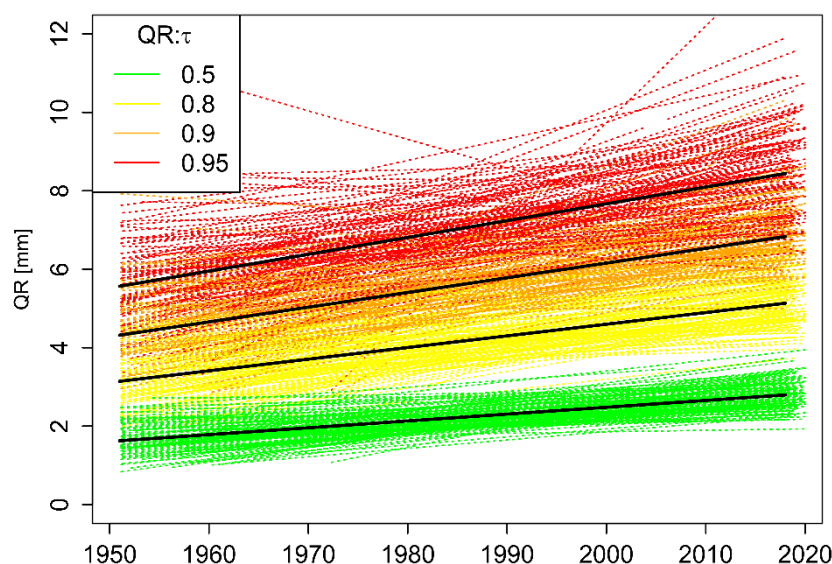


**Figure 4** Quantile regression (QR in mm) on monthly maximum 5 min rainfall intensities for the long series (LS) for different non-exceedance probabilities  $\tau$  (shown in coloured dashed lines and in the legend). The fitted quantile regression is shown with solid black line.

190 A test for trend, jump or stationarity based on in-stationary extreme value analysis (Coles, 2001) was performed for  
191 all 133 LS. We tested for linear trend in location parameter vs. jump at date of sensor change from analogue in early years  
192 to digital in the later years in the location parameter vs. stationarity. The decision was based on Akaike Information  
193 Criterion. The results for different duration levels (x-axis) are shown in **Figure 5** **Error! Reference source not found.** –  
194 left. It is obvious that the majority of instationarities at short duration levels is better explained as a jump (with mostly  
195 positive sign) in the data. A possible reason could lie in the limited ability of analogue gauges to register abrupt intensity  
196 changes, so that the total amount of precipitation falling in a short time interval may not be fully detected by analogue  
197 sensors, leading to positive jumps at sensor changes from analogue to digital. However, as a counter-argument, the so-  
198 called "step-response-error" that occurs with digital sensors could also be considered (see e.g. Licznar et al. (2015)). Since  
199 the instationarities are usually jumps and not trends, a simple homogenisation of the data to a uniform sensor type is  
200 possible by raising to the mean value of the digital sensor type (DVWK, 1999). This jump correction is applied separately  
201 for each station and duration level. The results of applying the instationarity test to the homogenised series are shown in

202 **Figure 5**– right. It can be seen that this approach can eliminate the instationarities at short duration levels significantly.  
 203 About 30% of the stations show instationarities (either trend or jump), while the remaining part is considered stationary.  
 204 Since only a small part of the stations show instationarities, here a stationary extreme value analysis is performed.

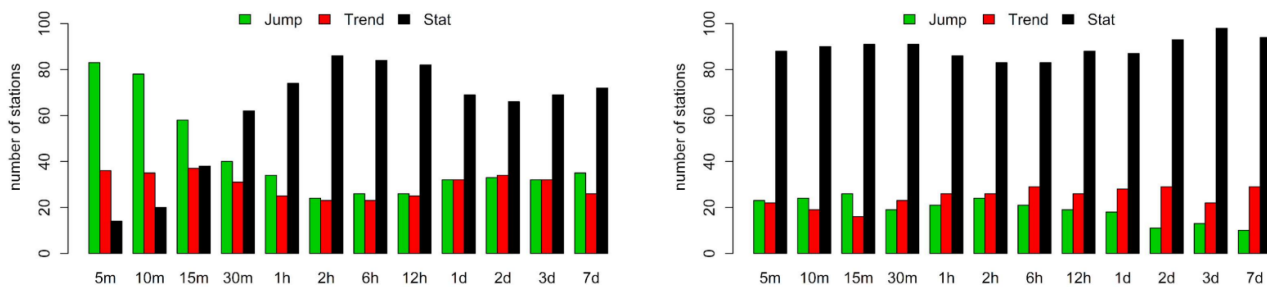


**Figure 5** Number of long series (LS) stations that show stationarity (stat) vs instationarity (either jump- or trend like) at different duration levels following the instationary extreme value analysis; left) before jump elimination and right) after jump elimination between analogue and digital sensors.

### 205 3. Methods

#### 206 3.1 Local Estimation of Extreme Value Statistics

##### 207 3.1.1 Reference Approach

208 Here, the Generalised Extreme Value (GEV) probability distribution is used for the statistical analysis of extreme  
 209 rainfall and the derivation of the local DDF curves, that is described as following:

$$210 \quad F(x; \mu, \sigma, \gamma) = \exp \left\{ - \left[ 1 + \gamma \frac{(x+\mu)}{\sigma} \right]^{-\frac{1}{\gamma}} \right\}, \quad 1 + \frac{\gamma(x-\mu)}{\sigma} > 0, \gamma \neq 0, \quad (1)$$

211 where  $\mu$  is the location,  $\sigma$  the scale and  $\gamma$  the shape parameter. If the shape parameter is greater than zero, heavy-tail  
 212 behaviour is present (GEV type II); if the shape parameter is less than zero, then it is the reverse Weibull distribution with  
 213 no-tail behaviour (Coles, 2001). The GEV parameters are fitted to the AMS of each duration level and station separately,  
 214 based on the L-moments method. For this purpose, the R-package “lmomco” was used (Asquith, 2021). A prior  
 215 investigation on our study revealed that the L-moment approach led to more stable results than the method of Maximum  
 216 Likelihood. The shape parameter was either estimated or fixed at 0.1 for estimation of return periods up to 100 years,  
 217 approximately following the recommendation from Koutsoyiannis (2004a, b) for estimation of return periods up to 100  
 218 years ( $\gamma \sim 0.1$ ) and on a prior analysis conducted on LS series. Based on the parameters obtained the quantiles of return  
 219 periods T1a, T10a, T20a, T50a and T100a were derived. Since the AMS-approach tends to underestimate quantiles at low  
 220 return periods ( $T_a < 10$  years), a correction of the AMS return periods according to the DWA 531-Regulations with factors  
 221 given in **Table 4** was performed.

**Table 4** Correction of the return periods ( $T_a$ ) when fitting the GEV to the Annual Maximum Series (AMS) adapted from DWA (2012).

Return Periods for POT	$T_a=1$ year	$T_a=5$ years	$T_a=10$ years
Return Periods for AMS	$T_a=1.6$ years	$T_a=5.5$ years	$T_a=10.5$ years



222 Because the parameters are fitted separately on each duration, quantile crossing may occur. Quantile crossing happens  
 223 when the extreme rainfall volumes of a fixed probability ( $T_a=100$  years) are not increasing with longer duration levels.  
 224 **Figure 6** shows for different return periods  $T_1a$ ,  $T_{10}a$ ,  $T_{20}a$ ,  $T_{50}a$  and  $T_{100}a$  the number of stations affected by these  
 225 crossings for the empirically calculated quantiles (left) and the quantiles fitted with the General Extreme Value (GEV)  
 226 distribution (right). The empirical quantiles are calculated according to Hyndman and Fan (1996). It is clear that the  
 227 number of stations with this problem increases significantly for larger return periods. In the empirical quantiles, especially  
 228 the SS show quantile crossing at long duration levels ( $D \geq 24h$ ). Here, the volumes of the duration  $D_{72h}$  and  $D_{168h}$  are  
 229 lower than the extremes of  $D_{24h}$ . With the GEV-fitted quantiles, significantly more stations show quantile crossings than  
 230 with the empirically calculated quantiles. These problems occur for all return periods, however are more frequent for the  
 231 return periods  $T_{50}a$  and  $T_{100}a$ . In order to avoid such problems two different methods are applied and compared here:  
 232 the approach presented by Koutsoyiannis et al. (1998) and the approach presented by Fischer and Schumann (2018).  
 233 These two methods are described below.

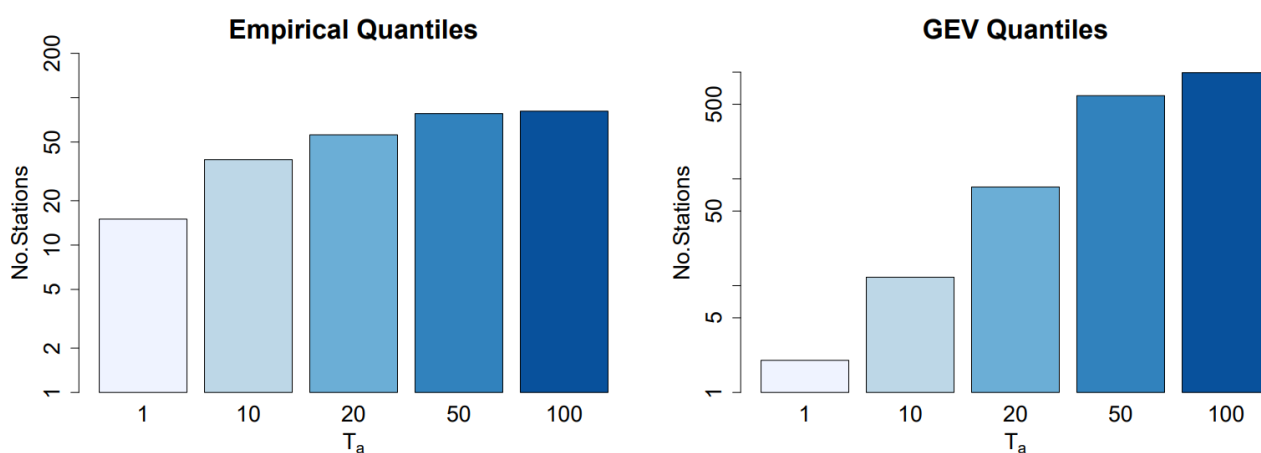


**Figure 6** Number of all stations at 5min resolution (for both short and long series) for different return periods ( $T_a$ ) showing quantile crossings in the empirically calculated quantiles (left) and the GEV-fitted quantiles (right) with increasing duration.

### 234 3.1.2 Koutsoyiannis Approach

235 Koutsoyiannis et al. (1998) considers the intensity as a function of the duration level through two parameters ( $\theta$ ,  $\eta$ ) and  
 236 the generalised intensity can be calculated from duration specific intensity as described below:

$$237 \quad i = i_d \cdot b_d \quad \text{with } b_d = (d + \theta)^\eta, \quad (2)$$

238 where  $i$  is the generalised intensity in mm/h,  $i_d$  is the intensity in mm/h observed at each duration level,  $d$  is the duration  
 239 level in hours and  $\theta$ ,  $\eta$  are the Koutsoyiannis parameters optimised for each station. Through this relationship a  
 240 generalisation of the AMS intensities over all the chosen duration levels is possible. The parameters  $\theta$  (larger than 0) and  
 241  $\eta$  (within the range 0 to 1) are estimated for each station by minimising the Kruskal-Wallis statistic as indicated in  
 242 Koutsoyiannis et al. (1998). The advantage of this optimisation method lies in its non-parametric character and robustness,  
 243 as the Kruskal-Wallis statistics is not affected by the presence of extreme values in the sample. Once the parameters  $\theta$   
 244 and  $\eta$  are determined, the generalised intensities from all duration levels are pooled together (as the main assumption is  
 245 now that they follow the same distribution) and a GEV distribution is fitted to this sample by the methods of L-moments.  
 246 Lastly, to obtain DDF curves, the quantiles at specific return periods are estimated from the fitted GEV distribution, and  
 247 are divided by the term  $b_d$  in Equation (2) (dependable on  $\theta$ ,  $\eta$  parameters and the duration level). This joint estimation of  
 248 parameters over all durations should not only avoid the quantile crossings, but also make the estimation of DDF more  
 249 robust.

250 3.1.3 Fischer/Schumann Approach

251 In contrast to Koutsoyiannis that treats the intensities of AMS as a function of the duration, Fischer and Schumann (2018)  
 252 propose an approach based on the GEV distribution, where the generalised GEV parameters are monotonically dependent  
 253 on the GEV parameters determined for each duration level. Thus, as a first step the GEV parameters (as in Equation (1))  
 254 are estimated from the L-moment methods for each duration level at each station, and then through a nonlinear regression  
 255 (with two parameters  $\alpha$  and  $\beta$ ) each GEV parameter is related to the different duration levels as indicated by the following  
 256 equations:

$$257 \mu_d = \frac{\alpha_\mu}{d^{\beta_\mu}}, \sigma_d = \frac{\alpha_\sigma}{d^{\beta_\sigma}} \text{ and } \frac{\sigma}{\gamma} = \alpha + \beta \cdot d, \quad (3)$$

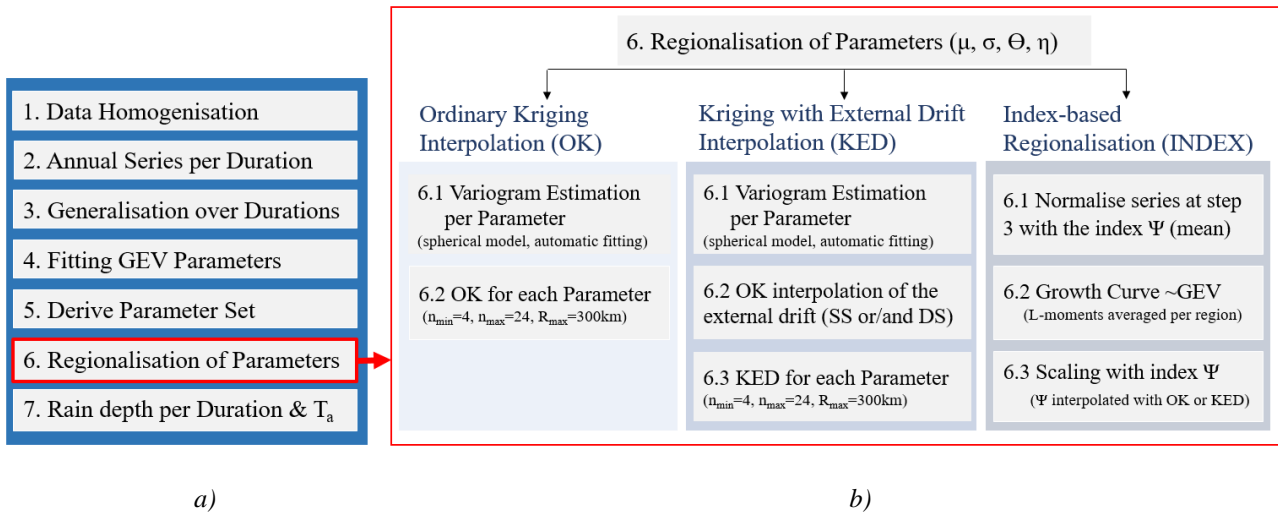
258 where  $d$  is the duration level in 5min,  $\mu_d, \sigma_d, \gamma$  are the GEV parameters of each duration, while  $\alpha$  and  $\beta$  are the regression  
 259 coefficients with  $\alpha_\mu, \alpha_\sigma > 0, \beta_\mu, \beta_\sigma > -1, \beta \geq 0$ . The parameters are obtained by nonlinear least-square-minimising. In  
 260 addition to the shape parameter dependency shown in Equation (3), three alternative approaches are considered: a constant  
 261 shape parameter over all durations, a shape parameter fixed at 0.1 and a quadratic relationship as in Equation (4).

$$262 \xi = a + P_1 \cdot \log(d) + P_2 \cdot \log(d)^2, \quad (4)$$

263 where  $P_1$  and  $P_2$  are estimated spanning across all stations and  $a$  is a station specific optimised parameter.

264 3.2 Regionalisation of Extreme Value Statistics

265 The local parameters estimated for each station (GEV parameters and generalisation parameters) make the base data set  
 266 for the regionalisation of the extreme rainfall statistics. Each of these parameters is regionalised independently based on  
 267 the regionalisation methods explained below, and later on, DDF maps for each duration and return period of interest are  
 268 generated. The overall procedure for regionalisation is given in **Figure 7-a**, and the regionalisation methods are given in  
 269 **Figure 7-b**. The regionalisation approaches were compared only for 4 parameters (see parameters of KO.FIX in **Table**  
 270 **5**), as these 4 parameters were selected as most appropriate for local DDF estimation in Section 4.1.



271  
272

**Figure 7** a) The step-by-step methodology applied here from the given point data sets to the final regionalised rainfall depths over all durations and return periods ( $T_a$ ) in Germany; b) a detailed procedure for Step 6 - Regionalisation (shown in red) only for the parameters of KO.FIX (see **Table 5**) carried out with different methods (ordinary kriging – left, external drift kriging – middle and index-based regionalisation – right). The parameters interpolated are the GEV (location -  $\mu$  and scale  $\sigma$ ) and Koutsoyiannis ( $\theta$  and  $\eta$ ) parameters. For both kriging methods, for each parameter first a spherical variogram is estimated (step 6.1) and the interpolation is performed (step 6.2 or 6.3) with the given  $n_{min}$ ,  $n_{max}$  and  $R_{max}$  which are the kriging parameters for minimum, maximum number of neighbours and maximum radius for neighbour

search. For index based regionalisation, first the generalised series obtained in step 3 are normalised with the index  $\Psi$  (step 6.1), next a regional GEV growth curve for each homogeneous region is derived based on regional L-moments (step 6.2) and finally the quantiles at each duration are re-scaled with the index  $\Psi$  (step 6.3).

### 273 3.2.1 Ordinary Kriging Interpolation

274 The regionalisation of extreme value statistics for Germany will first be carried out with Ordinary Kriging (OK)  
 275 interpolation. Here, the extreme rainfall parameters are interpolated independently. The flow chart for this interpolation  
 276 technique is shown in **Figure 7-b**. Ordinary Kriging is widely used for interpolation due to its simplicity in comparison  
 277 to other kriging methods. The expected value of the random process being investigation ( $E$ ) is treated as constant in space  
 278 (as per Equation (5)), whereas the increase in variance of the target variable at any two locations ( $u$  and  $u+h$ ) depends  
 279 only on the distance  $h$ . This increase in the variance is represented by the semi-variogram function  $\gamma(h)$  (here called  
 280 variogram). Therefore, in the first step, the empirical variogram is estimated by discrete point observations according to  
 281 Equation (6).

$$282 \quad E[Z(u+h)] = E[Z(u)] = m \quad (5)$$

$$283 \quad \gamma(h) = \frac{1}{2N(h)} \sum_{u_i - u_j = h} (Z(u_i) - Z(u_j))^2, \quad (6)$$

284 where  $N$  is the number of any two observed data pairs ( $u_i$  and  $u_j$ ) at distance  $h$ . Since the empirical variograms are not  
 285 continuous functions, theoretical variograms must be fitted to the observed values. To describe the spatial variance of the  
 286 data, several theoretical variogram models can be used and fitted to the empirical variogram using the least squares  
 287 method. For the interpolation of rainfall extremes a spherical variogram (as per Equation (7)) is chosen as more  
 288 appropriate (Kebaili Bargaoui and Chebbi, 2009).

$$289 \quad \gamma(h) = c_0 + c \cdot \left( \frac{3h}{2a} - \frac{h^3}{2a^3} \right) \text{ for } h \leq a \text{ and } \gamma(h) = c \text{ for } h = a, \quad (7)$$

290 where  $c_0$  is the nugget,  $c$  the sill and  $a$  the range of the variogram. The variogram describes the spatial variability of the  
 291 target variable and the average dissimilarity between a known and unknown location. Once the theoretical variogram is  
 292 known, it can be used as a basis for interpolating the statistical properties on a 5km grid. This grid resolution was chosen  
 293 for two reasons; first it is consistent with the HyRas product from German Weather Service that uses the same resolution,  
 294 second it is a compromise between the coarsest and finest legible resolution computed from the given density of long  
 295 series (LS) (the reference for this study) following the suggestions of Hengl (2006). The interpolation is done as indicated  
 296 in Equation (8), the variable at an unknown location ( $Z'$ ) is estimated by the weighted average of the nearby known  
 297 locations ( $Z_{u_i}$ ).

$$298 \quad Z'(u_o) = \sum_{i=1}^n \lambda_i \cdot Z(u_i), \quad (8)$$

299 where the weights ( $\lambda_i$ ) are derived from the theoretical variogram, and  $n$  is the number of selected neighbours. The R-  
 300 package "gstat" is used to fit the variograms and interpolate the variables (Pebesma, 2004). An advantage of Ordinary  
 301 Kriging interpolation is that the weights are determined in such a way that the difference between the estimate and the  
 302 observed values is zero on average. However, this can lead to the interpolated variable being smoothed in space. Different  
 303 theoretical variograms were previously investigated, i.e. exponential, gaussian and spherical, with the spherical model  
 304 together with a nugget effect showing the best fit for the case study. The fitting of the variogram model parameters for  
 305 different data types and experiments is done automatically by weighted least square fit. Since the automatic fit relies on  
 306 the initial values of the model parameters, we defined the initial values with trial and error, and accepted a fit that was  
 307 adequate qualitatively. **Figure 8** illustrates the empirical and theoretical normalised variograms for interpolation of the

308 GEV and Koutsoyiannis parameters (after method KO.FIX shown in **Table 5**) estimated from the three main datasets  
309 available: long series (LS), short series (SS) and 30 realisations of disaggregated daily series (DS). Note that the  
310 variograms are normalised in order to ensure a comparison between the different datasets. From this figure a clear  
311 difference between the spatial dependency of different datasets, due to different station densities and settings, is visible.  
312 The long and short series (LS and SS) exhibits similar relationship with each other for the GEV parameters ( $\mu$  and  $\sigma$ ) but  
313 distinguish either in the nugget value ( $c_0$ ) or the range ( $a$ ), whilst the daily disaggregated series clearly exhibit different  
314 nugget ( $c_0$ ), range ( $a$ ) and even sill ( $c$ ). The differences between the datasets are less visible in the spatial dependencies  
315 of the Koutsoyiannis parameters ( $\theta$  and  $\eta$ ), where the three datasets differ slightly in nugget and range. Particularly the  
316 spatial dependency of the scale parameter is captured quite differently by the three datasets. Here, LS and SS are differing  
317 mainly at the nugget value, where LS has a smaller value than the SS series suggesting that the spatial structure of the  
318 scale parameter from SS is smoother than that of LS. On the other hand, the DS datasets exhibit a completely different  
319 variogram for the scale parameter, suggesting that the extremes of high return period (influenced mainly by the scale  
320 parameter) will have different spatial structures than those of LS and SS series.

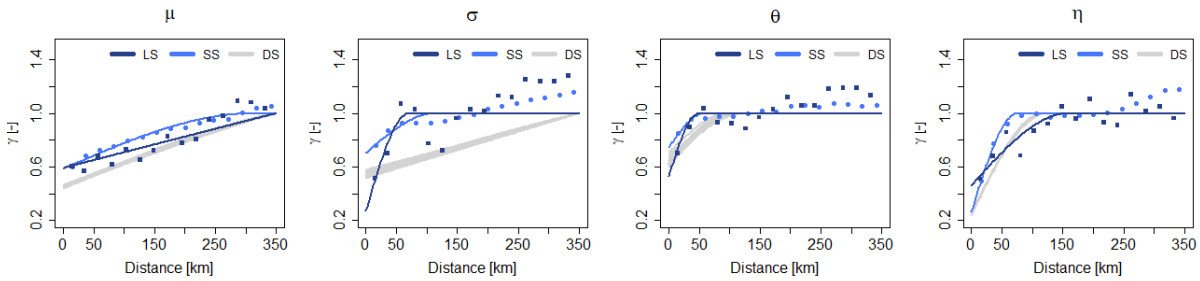


**Figure 8** Empirical (dots) and fitted (solid lines) spherical theoretical variograms for the GEV ( $\mu$  - location and  $\sigma$  - scale) and Koutsoyiannis ( $\theta$  and  $\eta$ ) parameters estimated by three different datasets (long series LS in dark blue, short series SS in light blue and disaggregated daily series DS in grey).

### 3.2.2 Kriging with External Drift Interpolation

322 In the Kriging with External Drift (KED), the expected value  $E$  of the target variable  $Z$  at any location  $u$  is linear dependent  
323 on secondary variables  $Y$ , and thus the Equation (5) takes the form of the Equation (9). Here the secondary variables (or  
324 the external drifts) reflect the spatial trend of the target variable. Theoretically, the variogram for KED interpolation is  
325 computed from the residuals between the target and the secondary variables. Here, for simplicity the OK variograms are  
326 used instead, since as shown in Delrieu et al. (2014) they can produce very similar results to the KED one.

$$327 \quad E[Z(u) | Y_1(u), Y_2(u), \dots, Y_m(u)] = b_0 + \sum_{k=1}^m b_k Y_k(u) \quad (9)$$

328 where  $Y$  represent  $k$  secondary variables from 1 to  $m$  that are used as an external drift,  $b_0$  in the interception of the linear  
329 dependency and  $b_k$  the coefficient for each  $k$  drift. For this study different site characteristics (i.e. elevation) were  
330 investigated as external drift, however as indicated by the cross-correlation between the target variables (in this case the  
331 4 parameters describing the local statistics) and the site characteristics, the linear dependency between them is not high  
332 (see in appendix **Figure A1**). Therefore, here only interpolated local parameters from the short and/or daily series are  
333 used as external drift information.

334 3.2.3 Index-based Regionalisation

335 The regionalisation of extreme rainfall statistics in Germany is as well carried out using the index method according to  
336 Hosking and Wallis (1997). The index method was originally developed for the regionalisation of flood quantiles,  
337 however found a wide application also for the regionalisation of extreme rainfall statistics. By pooling information in  
338 statistically homogeneous regions, a more robust estimate of extreme rainfall statistics can be made and based on each  
339 defined region, the information can be transferred to other unobserved points. A homogeneous region exists if the  
340 distribution functions have the same shape at all points in the region. The homogeneity indicator  $H_1$  presented by Hosking  
341 and Wallis (1997) is typically used to determine homogeneous regions. If the  $H_1$  is lower than 1, the region is said to be  
342 homogeneous, if it is between 1 and 2 the region may be heterogeneous, and else, if it is higher than 2, the region is  
343 definitely not homogeneous. Here different site characteristics like the latitude, longitude, elevation, long term annual  
344 average of sunshine duration and mean annual precipitation were used as input to define homogeneous regions. Based on  
345 a k-clustering approach (Ward, 1963) nine homogeneous regions were identified and are shown in **Figure 9**  
346 **Reference source not found.** The obtained homogeneous regions were tested for homogeneity for each data type  
347 combination and, as visible from **Figure A2** in appendix, all values are below 1, meaning that the regions selected are  
348 homogeneous and can be used for the index-based regionalisation. Note that the generalised statistics over all the durations  
349 from Section 3.1 are used as input for the homogeneity test. The R-package “nsRFA” is used to obtain the homogeneous  
350 regions (Viglione et al., 2020). In order to find an appropriate number of clusters, different number of clusters between 2  
351 and 20 are tested and compared based on the homogeneity indicator  $H_1$  and whether they were spatially continuous and  
352 physically reasonable. The maximum number of clusters of 20 was chosen to ensure a sufficient number of stations and  
353 thus a sufficient number of observation years per region (Hosking and Wallis, 1997).

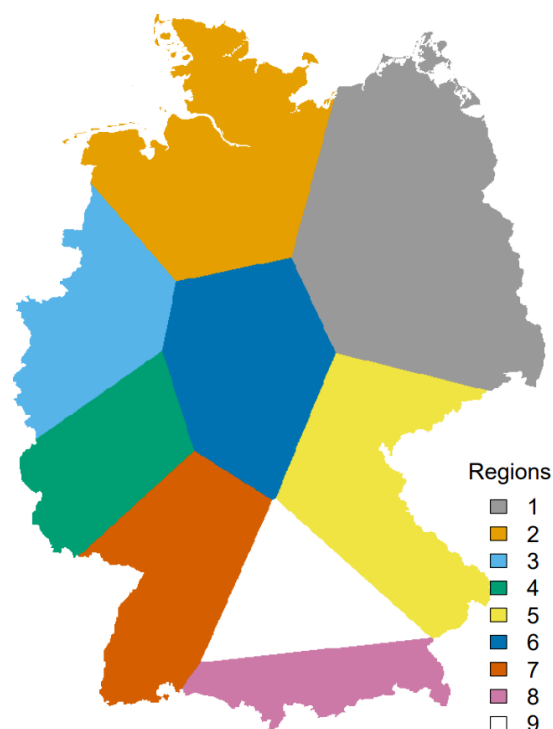


**Figure 9** Nine homogeneous regions implemented here for the index-based regionalisation. The regions shown here are a generalisation of the k-cluster results to account for spatial consistency.

354 Once the homogeneous regions are determined, the different local statistics are normalised by a scaling factor, the index.  
355 In contrast to the previous regionalisation techniques discussed so far, the index-based regionalisation has an extra step –  
356 the normalisation of the general intensities with the index (performed at step 3 in **Figure 7** – left), which in this case is

357 the mean generalised intensity. Next, the local L-moments are estimated on the basis of the normalised annual series and  
 358 regional L-moments are derived for each region weighting the local L-moments according to their time series length.  
 359 Finally, a GEV growth curve is fitted for each region via the regional L-moments. The R-package “lmomRFA” was  
 360 employed for the application of the index method (Hosking and Wallis, 1997). In the final step, by back-scaling the  
 361 normalised extreme rainfall for all observed and unobserved points in the homogeneous region, estimates can be made  
 362 about the extreme rainfall as a function of the duration (based on regional averaged values of observed  $\theta$  and  $\eta$ ) and the  
 363 return period (based on regional GEV growth curve). The geostatistical interpolation of the index makes it possible to  
 364 transfer the extreme value statistical evaluations to unobserved points within the region.

### 365 3.3 Performance Assessment and Comparison

#### 366 3.3.1 Local Performance Assessment

367 For the local estimation of the GEV parameters that describe the extreme rainfall over all the selected duration levels, two  
 368 different approaches were consulted: from Koutsoyiannis et al. (1998) (herein referred as KO) and from Fischer and  
 369 Schumann (2018) (herein referred as FS). Before carrying on with the regionalisation it is important to investigate which  
 370 of the methods is more adequate for the estimation of the GEV parameters over all the duration levels. Moreover, the two  
 371 methods do not only distinguish in their approach of generalisation across duration, but they also include different  
 372 variations on the calculation of the GEV shape parameter ( $\gamma$ ). A review of the methods and shape parameters is given in  
 373 **Table 5**, together with the respective optimised parameter set for each case. The obtained parameters for different data  
 374 sets are shown in the appendix: **Figure A3** for KO and in **Figure A4** for FS.

*Table 5 A review of the methods and the different calculation of the shape parameter investigated for the local statistics, where KO stands for the Koutsoyiannis and FS for the Fischer and Schumann framework.*

Method	Shape Parameter	Abbreviation	Optimised Parameter
KO	is constant per each station, as fitted by L-moments	KO.CON	$\mu, \sigma, \gamma, \theta, \eta$
	is fixed at all stations as $\gamma = 0.1$	KO.FIX	$\mu, \sigma, \theta, \eta$
FS	is calculated as proposed by Fischer and Schumann	FS.RLM	$\alpha_\mu, \beta_\mu, \alpha_\sigma, \beta_\sigma, \alpha, \beta$
	is constant over all durations	FS.CON	$\alpha_\mu, \beta_\mu, \alpha_\sigma, \beta_\sigma, \gamma$
	a quadratic dependence on duration specific shape	FS.QUA	$\alpha_\mu, \beta_\mu, \alpha_\sigma, \beta_\sigma, a$
	is fixed at all stations as $\gamma = 0.1$	FS.FIX	$\alpha_\mu, \beta_\mu, \alpha_\sigma, \beta_\sigma$

375 The performance of the methods and the respective case of shape parameters as illustrated in **Table 5** is evaluated only  
 376 at the location of the long series (LS) by comparing the normalised quantiles over all durations for return periods T1a,  
 377 T10a, T20a, T50a and T100a with the GEV quantiles calculated separately at each duration level. Here the percentage  
 378 RMSE (as per Equation (10)) was employed to assess the errors of the selected cases at each duration level and station  
 379 with respect to the GEV duration specific quantiles:

$$380 \quad \text{Percentage RMSE:} \quad RMSE_{d,st} [\%] = 100 \cdot \frac{\sqrt{\frac{1}{5} \sum_{i=1}^5 (RD_{gen,st} - RD_{d,st})^2}}{\overline{RD}_{d,st}}, \quad (10)$$

381 where  $i$  represents each of the 5 selected return period  $T_a$  varying from 1 to 100 years,  $st$  varies from 1 to 133 available  
 382 long series,  $RD_{gen,st}$  corresponds to the derived rainfall depth from the generalisation method of duration  $d$ ,  $RD_{d,st}$  the  
 383 derived rainfall depth from the GEV quantiles at duration  $d$ , and the  $\overline{RD}_{d,st}$  is the mean rainfall depth from the GEV  
 384 quantiles at a duration  $d$  averaged over the return periods. Alternatively, the error for each return period and station can  
 385 as well be calculated by Equation (10) by swapping the  $d$  with  $T_a$ , and where  $\overline{RD}_{T_a,st}$  is the mean rainfall depth from the

386 GEV quantiles at return period  $T_a$  averaged over the duration levels  $d$  (from 5min up to 7d, therefore  $i$  changes from 1 to  
387 12).

388 Since the GEV quantiles fitted per each duration level cannot be considered the ground truth, a non-parametric bootstrap  
389 is performed when estimating the parameters of each method, in order to investigate the sampling uncertainty of derived  
390 DDF values. For this purpose, 100 randomisations of the observations were conducted and the uncertainty range of the  
391 derived rainfall depths is computed as following:

$$392 \quad \text{Normalised 95\% Confidence Interval Width:} \quad nCI95_{width}[-] = \frac{CI95_{st,d,Ta}}{Mean_{st,d,Ta}} \quad (11)$$

393 where  $nCI95_{width}$  is the 95% confidence interval width and  $Mean$  is the average of rainfall depth obtained from 100  
394 realisations and expressed for each long series (LS) location  $st$ , duration level  $d$  and return period  $T_a$ . The smaller the  
395 uncertainty range, the more robust are the estimated parameters for the high return periods. Based on the two performance  
396 criteria, percentage RMSE and  $nCI95_{width}$ , all the methods in **Table 5** are compared to evaluate the best one for the  
397 estimation of rainfall DDF curves. The best method is selected as the one with the lowest RMSE and  $nCI95_{width}$ . The  
398 results of this comparison are given in Section 4.1.

### 399 3.3.2 Spatial Performance Assessment

400 In order to check which of the regionalisation approaches provides the best results, a leave-one out cross-validation was  
401 carried out at the locations of the long series (LS 133 stations). For each approach, the rainfall depth (RD) is determined  
402 from the return periods T1a, T10a, T20a, T50a and T100a and the selected duration levels. After regionalisation, the  
403 regionalised rainfall depths are compared with the local generalised GEV quantiles (here assumed to be the truth). The  
404 short series are omitted from the cross-validation, as no reliable extreme value statistics can be carried out for large return  
405 periods due to the very short observation length. The quality of the regionalisation approaches is evaluated using the  
406 following criteria:

$$407 \quad \text{Percentage Bias:} \quad PBIAS_{st,Ta}[\%] = 100 \cdot \frac{\frac{1}{D} \sum_{d=1}^D (RD_{regional,d} - RD_{local,d})}{\sum_{d=1}^D (RD_{local,d})}, \quad (12)$$

$$408 \quad \text{Percentage RMSE:} \quad RMSE_{st,Ta}[\%] = 100 \cdot \frac{\sqrt{\frac{1}{D} \sum_{d=1}^D (RD_{regional,d} - RD_{local,d})^2}}{\overline{RD_{local}}}, \quad (13)$$

$$409 \quad \text{Nash-Sutcliffe Criteria:} \quad NSC_{st,Ta}[-] = 1 - \frac{\sum_{d=1}^D (RD_{regional,d} - RD_{local,d})^2}{\sum_{d=1}^D (RD_{local,d} - \overline{RD_{local}})^2}, \quad (14)$$

410 where the  $d$  varies from 1 to  $D=12$  for each duration level between 5min and 7days,  $T_a$  the return period,  $st$  the respective  
411 long series (LS) station,  $RD_{regional}$  corresponds to the regionalised rainfall depth,  $RD_{local}$  the locally derived rainfall depth  
412 from the generalised GEV function and the  $\overline{RD_{local}}$  is the mean local rainfall depth averaged over the durations. The  
413 cross-validation only at the location of the LS makes it possible to investigate the value that the short (SS) and the  
414 disaggregated daily series (DS) are adding to each regionalisation method. For this purpose, the regionalisation methods  
415 are run first only with the LS as input, and the performance of such an application is considered the benchmark for  
416 improvement. Later on, the SS and DS are added stepwise as input to the regionalisation, in order to assess the  
417 improvement, they introduce towards the benchmark. Additionally, one can calculate the expected performance when  
418 only the short or/and the disaggregated daily series are available, and not the long one. An overview of these experiments  
419 and their aim is given at **Table 6**.

**Table 6** Overview of the experiments performed with different data sets for each regionalisation method, where SS – are short series, LS – long series and DS – disaggregated daily series.

Input	Aim
Only LS	Benchmark for improvement
Only SS	The expected error from only short series
Only DS	The expected error from only disaggregated daily series
LS and SS	The added value from the short series
LS and DS	The added value from the daily disaggregated series
SS and DS	The expected error from short and daily disaggregated series
LS, SS and DS	The added value from the short and daily disaggregated series

420 A directed comparison of the performance criteria between the different experiments and the benchmark is calculated  
421 here as per Equation (15).

$$422 \quad Perf_{impr,Ta} [\%] = 100 \cdot \frac{(-Perf_{new,Ta} + Perf_{ref,Ta})}{Perf_{ref,Ta}}, \quad (15)$$

423 where  $Perf_{ref,Ta}$  is the performance criteria calculated for each return period  $Ta$  as per Equation (12)-(14) from the scenario  
424 with only LS as input, and  $Perf_{new,Ta}$  is the performance of any other combination of input data as per Equation (12)-(14).  
425 A positive value for this criterion indicates an improvement in performance in comparison to the only LS scenario, while  
426 a negative value indicates a deterioration. Note that, the signs of the nominator are exchanged in the case of the  
427 improvement of the NSE. It is as well important to emphasise that the scenario *ref* corresponds to the best regionalisation  
428 method with only LS as input, namely ordinary kriging of LS based on results of Section 4.2.

429 Finally, based on different combinations of the available series (data types) as external drift in the kriging interpolation  
430 may help to shed light on which combination of the data is more useful for the regionalisation of the rainfall DDF values.  
431 Here the data to be used as external drift are first interpolated with ordinary kriging. A description of these different  
432 combinations for the KED interpolation is given in **Table 7**. The performance of the different combinations is evaluated  
433 only at the location of the LS, and the best integration is selected based on the highest improvement in comparison to  
434 regionalisation with only LS as input.

**Table 7** Overview of different integration of data types in Kriging with External Drift (KED) interpolation where SS – are short series, LS – long series and DS – disaggregated daily series. Pooling the data together with same importance is represented by (+) sign, whereas priority importance (integration through an external drift) is represented by the (|) sign.

Combination	Abbreviation
Interpolate LS with OK[SS] as external drift	KED[LS SS]
Interpolate LS with OK[DS] as external drift	KED[LS DS]
Interpolate LS with both OK[SS] and OK[DS] as external drift	KED[LS SS+DS]
Interpolate LS and SS with OK[DS] as external drift	KED[LS+SS DS]
Interpolate SS with OK[DS] as external drift	KED[SS DS]

435



436 **4. Results**

437 **4.1 Local Estimation of Extreme Statistics**

438 **Figure 10** illustrates the local percentage RMSE of each method in comparison to the duration specific quantiles (as per  
 439 Equation (10)). The upper row of **Figure 10** shows the percentage RMSE calculated for each location and duration level  
 440 over all the return periods and the lower row of **Figure 10** shows the percentage RMSE calculated for each location and  
 441 return period over all the duration levels. The results from **Figure 10** – upper row indicate that the KO approaches (both  
 442 fix and station constant shape parameter) have an almost constant RMSE over all durations under the value 10%. On the  
 443 other hand, the FS approaches tend to have similar or little smaller RMSE for the longer duration (median RMSE under  
 444 8%), but are not able to represent well enough the very short durations. For the FS approaches, the RMSE median for  
 445 duration levels up to 60 min, is higher than 10%, with the 5min RMSE being the highest (between 25-45%). The results  
 446 from **Figure 10** – lower row illustrate that all the approaches manifest higher errors with higher return period. Both of the  
 447 KO approaches (fix and station constant shape) show very similar behaviour. The KO.FIX performs slightly worse (1-  
 448 4% higher RMSE) than the KO.CON, but this is expected as the duration GEV fitted per each duration independently  
 449 favours the KO.CON (as the shape parameter is let free for the GEV parameter fitting). The FS approaches perform very  
 450 similarly to one another, however here contrary to the KO.FIX approach, the performance of the FS.FIX seems better  
 451 than the other approaches. Overall, the KO approaches have the priority at shorter durations and they can capture the  
 452 volumes at specific durations better than the FS approaches. On the other side, the FS approaches can capture better  
 453 extremes at longer durations. A unanimous selection is not yet possible from the obtained results so far, because the local  
 454 GEV duration specific parameters may not represent the ground truth.

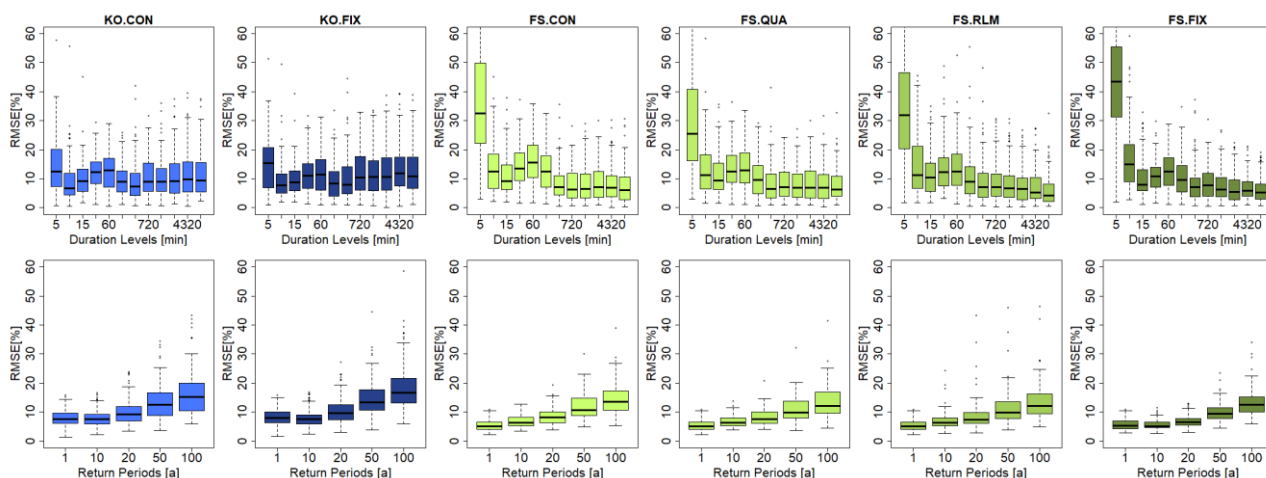
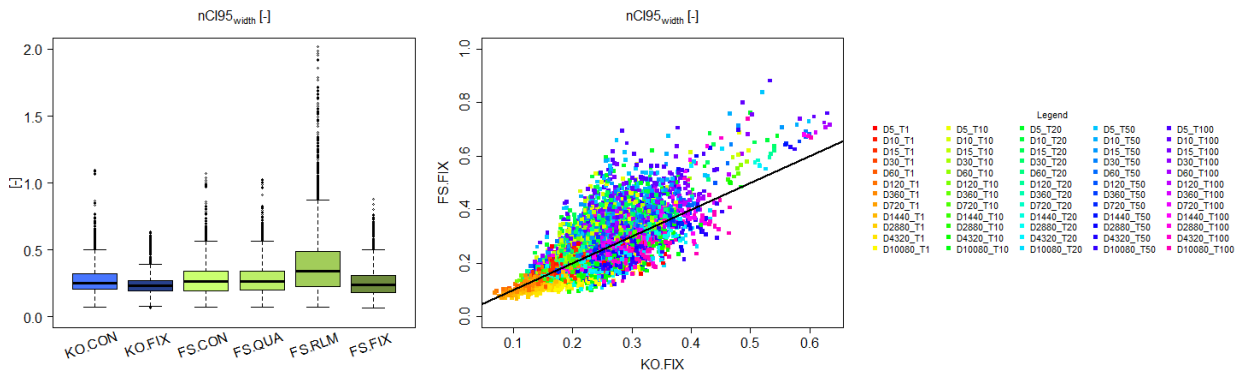


**Figure 10** RMSE (%) performance of the given generalisation methods over all the long series (LS) in comparison to the duration specific GEV quantiles grouped: upper row - for different duration levels (calculated per station over return periods  $T_a$ ), and lower row - for different return periods (calculated per station over duration levels). The overview of the methods shown here is given in Table 5.

455 To analyse which approach estimates more stable and representative parameters, a non-parametric bootstrap was  
 456 performed (with 100 random realisations), and served as a basis for assessing the 95% confidence interval width of the  
 457 obtained DDF values. **Figure 11**-left shows the normalised 95% confidence interval widths ( $nCI95_{width}$ ) for the rainfall  
 458 depth (as per Equation (11)) estimated for each of the selected approaches. A high value of the  $nCI95_{width}$  indicates that  
 459 the bootstrap yields very variable rainfall depths, and hence a higher uncertainty is associated with the method. Contrarily  
 460 a low value of the  $nCI95_{width}$  indicates that the rainfall depths have low variation across the random realisations, and thus  
 461 the obtained DDF curves are considered more stable or robust. The results shown in **Figure 11** indicate that the KO.FIX  
 462 exhibits the lowest variation (median  $nCI95_{width} \sim 0.23$ ), followed up by FS.FIX ( $\sim 0.25$ ), and by KO.CON, FS.CON,

463 FS.QUA with slightly higher variations (respectively  $\sim 0.3$ ). Interesting is to see that the FS.RLM has a median  $nCI95_{width}$   
 464  $\sim 0.3$  but can reach extreme values up to 2. **Figure 11-right)** shows the scatterplot of  $nCI95_{width}$  obtained from the KO.FIX  
 465 (x-axis) and FS.FIX (y-axis) for different duration levels and return periods (shown with different colours) at the LS  
 466 locations. Except for very low return periods (T1a), FS.FIX exhibits on average higher values of  $nCI95_{width}$  than KO.FIX.  
 467 Based on these results, the KO.FIX (Koutsoyiannis framework with shape parameter fixed at 0.1) was chosen as the best  
 468 method and was used for the regionalisation of the DDF curves. The advantages of the KO.FIX are that: 1. It represents  
 469 all duration levels similarly and fairly, 2. The parameter estimation is more robust than any of the other methods, 3. It  
 470 uses a known and well-established method for the estimation of the DDF curves.

471



472

**Figure 11** left) comparison of the normalised 95% confidence interval width [-] for the methods and shape parameters selected for the generalisation of the DDF values over all the durations (see Table 5 for a summary of the methods); right) a direct comparison of the normalised 95% confidence interval width [-] for KO.FIX (x-axis) with FS.FIX (y-axis) for each duration  $D$  and return period  $T$  (shown in different colours).

#### 473 4.2 Regionalisation of Extreme Statistics

474 As discussed in the Section 4.1, the AMS at different duration levels were normalised according to Koutsoyiannis  
 475 approach and the GEV parameters were fitted to the grouped generalised intensities. The shape parameter was kept fixed  
 476 at 0.1. Ordinary Kriging (OK) and index-based (INDEX) regionalisation were run first only with the LR data as input –  
 477 to decide about which of the two approaches will serve as a benchmark. A direct comparison based on Equation (15) is  
 478 then performed for each of the selected performance criteria (where *new* is OK and *ref* is INDEX), to compute the  
 479 improvement or deterioration of OK with only LS data compared to the INDEX. The median values for each return period,  
 480 performance criteria and method, are given in **Table 8**. Here it becomes clear that the kriging approach exhibits lower  
 481 RMSE for all return periods, worse BIAS for high return periods, and slightly better NSE than the index method. Based  
 482 on these results, the kriging with LS as input (KRIGE[LS]) is used as a benchmark for calculating the improvement in  
 483 performance by adding additional data types. Apart from the performance, the other advantage of kriging is that it is more  
 484 of a “pure” method, as it interpolates independently the 4 parameters, while the index approach is a “mixture” between  
 485 the regional growth curve estimation, averaging  $\theta$  and  $\eta$  parameters, and kriging to interpolate the index. For this reason,  
 486 one may prefer the kriging regionalisation, as the errors are mainly from the kriging system, while the index method  
 487 includes errors from the kriging system and from regional and averaged parameters.

**Table 8** Median performance improvement/deterioration (%) of ordinary kriging (OK) versus index-based (INDEX) regionalisation calculated for different data as per Equation (15) (where *new* is OK and *ref* in INDEX), when only long

series (LS) are used as input. The performance is obtained by cross-validation over 133 LS stations. The colour green (+) indicates better performance by OK, red (-) indicates better performance by INDEX.

488

	RMSE (%)					PBIAS (%)					NSE (%)				
	T1a	T10a	T20a	T50a	T100a	T1a	T10a	T20a	T50a	T100a	T1a	T10a	T20a	T50a	T100a
LS	5.270	1.230	-0.268	0.015	1.510	2.500	-1.200	-1.440	-3.440	-2.469	0.250	0.010	0.002	0.002	0.006

489

#### 4.2.1 Best Regionalisation for Different Data Combination

490

Kriging and index-based regionalisation was then performed for each data type experiment given in **Table 6**, and the cross-validation results for the 133 LS locations were compared to the benchmark (KRIGE[LS]) selected before as the best regionalisation with only LS as input. To enable an easy comparison between the two regionalisation methods, the difference between the improvements achieved between the kriging and the index-based regionalisation in comparison to the benchmark was calculated for each of the 133 LS locations. The median differences (in percent) for each data type experiment over the 133 locations for each performance criteria and return period are given in **Table 9**. A positive difference (dark green shade) means that the improvements reached by the kriging interpolation are higher than the index-based regionalisation. A negative difference (red shade) means the opposite. The data are combined by two operators: either (+) referring to pooling of the datasets together with same importance (the parameters and the index are interpolated with ordinary kriging), and (|) referring to a linear relationship between the datasets (priority importance) where the parameters and the index are interpolated through external drift kriging.

500

**Table 9** Median difference between kriging and index-based improvements calculated for different data as per Equation (15). The median is computed from 133 stations. The data used as input are short series (SS), long series (LS) and disaggregated daily series (DS) and combined either with same importance (+) or with priority importance (|). The positive difference shown in green shades indicate that kriging introduces bigger improvements towards the benchmark than the index-based regionalisation. The negative differences shown in red shades indicate that the index-based regionalisation has the bigger improvements.

501

	RMSE (%)					PBIAS (%)					NSE (%)				
	T1a	T10a	T20a	T50a	T100a	T1a	T10a	T20a	T50a	T100a	T1a	T10a	T20a	T50a	T100a
SS	15.1	8.2	9.6	-0.1	0.4	6.5	10.4	4.8	1.5	-2.3	-0.1	0.6	0.0	0.0	-0.1
DS	19.4	4.8	6.1	10.1	12.2	-2.6	2.9	8.0	11.5	11.8	0.4	0.3	0.8	0.8	0.9
LS+SS	8.3	3.6	6.4	-2.3	-0.8	8.0	3.5	0.2	-6.7	-11.4	0.3	0.2	0.2	0.2	-0.1
LS SS	5.5	11.6	12.3	9.8	10.8	13.0	8.6	3.6	6.1	6.0	0.2	0.3	0.5	0.5	0.5
LS+DS	101.2	90.4	75.3	77.3	76.9	157.5	162.9	154.7	134.1	130.5	10.1	10.0	10.1	10.1	10.0
LS DS	20.7	16.6	16.1	15.5	12.8	27.6	12.6	10.5	3.9	1.4	0.7	0.4	0.4	0.4	0.3
SS+DS	111.0	97.5	82.5	79.0	82.6	176.0	194.6	188.7	157.2	150.8	10.3	9.8	9.8	9.8	9.4
SS DS	10.6	6.8	8.8	4.0	5.1	9.9	-3.4	-2.8	-2.3	-5.9	0.2	0.4	0.3	0.3	0.2
LS+SS+DS	59.8	44.1	45.5	43.3	41.4	110.4	132.6	141.8	109.7	107.3	5.1	4.6	4.4	4.4	4.1
LS+SS DS	13.1	12.2	13.2	10.6	11.9	10.4	2.0	-0.8	1.0	-2.8	0.2	0.5	0.5	0.5	0.5
LS SS+DS	20.1	13.3	11.5	6.1	3.3	18.2	8.1	8.1	-0.2	-1.9	0.5	0.3	0.2	0.2	0.1

502

The results from the **Table 9** indicate that for most of the cases the kriging interpolation brings higher improvements to the benchmark than the index-based regionalisation. Exceptions are the regionalisation with only SS, LS+SS, SS|DS, LS+SS|DS and LS|SS+DS where the index-based regionalisation exhibits on median 2-12% higher PBIAS improvement for higher return periods than the kriging interpolation. However, for these cases, the RMSE and the NSE improvements are much higher for the kriging regionalisation. Therefore, it can be concluded that overall, the kriging interpolation yields better results than the index-based regionalisation (lower RMSE and higher NSE), but may suffer depending on the combination of data types from slightly higher PBIAS. Also, it has to be mentioned, that when grouping the daily disaggregated time series directly (operator +) with the other data types (either LS and SS), the kriging performs up to

509

510 100% better than the index-based regionalisation. This suggests that the parameters from the disaggregation do not follow  
 511 the same regions or growth curve as the high-resolution data (LS and SS), thus a kriging interpolation seems a more  
 512 reasonable choice for integrating daily disaggregated series (DS).

513 The results of **Table 9** give a direct comparison between kriging and index-based regionalisation, nevertheless as they  
 514 are relative to each case, do not give any information if ordinary kriging or external drift kriging is yielding better  
 515 regionalisation results. For this purpose, the difference of improvements between KED and OK were calculated and  
 516 shown as median over the 133 LS locations in **Table 10**. A positive difference (green shade) means that the improvements  
 517 reached by KED are higher than the OK interpolation. A negative difference (red shade) means otherwise. The results  
 518 show that overall, the KED exhibits higher RMSE and NSE improvements than the OK, but the KED tends to have lower  
 519 PBIAS improvements than the OK. When only the high-resolution data sets are present (LS and SS), the KED behaves  
 520 better than OK mainly for high return periods (50-100a), when LS and DS are present, KED clearly outperforms the OK.  
 521 For all the remaining cases the OK outperforms the KED only for the PBIAS of high return periods.

**Table 10** Median difference between external drift kriging (KED) and ordinary kriging (OK) improvements calculated for different data as per Equation (15). The median is computed from 133 stations. The data used as input are short series (SS), long series (LS) and disaggregated daily series (DS) and combined either with same importance (+) or with priority importance (/). The positive difference shown in green shades indicate that KED introduces bigger improvements towards the benchmark than the OK. The negative differences shown in red shades indicate that the OK regionalisation has the bigger improvements.

	RMSE (%)					PBIAS (%)					NSE (%)				
	T1a	T10a	T20a	T50a	T100a	T1a	T10a	T20a	T50a	T100a	T1a	T10a	T20a	T50a	T100a
LS and SS	-6.4	2.0	-1.9	7.8	8.8	-1.3	-4.9	-5.2	1.2	6.2	-0.5	-0.2	0.1	0.1	0.5
LS and DS	56.4	41.0	39.4	32.9	30.2	57.6	30.5	20.7	14.5	13.2	2.5	1.7	1.6	1.6	1.5
SS and DS	46.4	30.5	27.2	26.3	27.8	37.1	1.0	-8.1	-11.3	-14.9	1.9	1.4	1.3	1.3	1.4
LS+SS/DS	42.2	20.2	19.7	17.4	20.2	39.3	-0.5	-16.0	-18.6	-19.9	1.8	1.2	1.0	1.0	1.2
LS SS+DS	40.0	20.6	16.3	16.4	16.4	37.0	-2.5	-21.5	-16.8	-17.7	1.6	1.0	0.9	0.9	1.0

#### 523 4.2.2 Best Data Integration for Regionalisation

524 So far, the external drift kriging interpolation has shown superiority for regionalising DDF curves in comparison to the  
 525 index-based and ordinary kriging regionalisation. Nevertheless, the question still remains, what is the best combination  
 526 of the data sets for regionalising the DDF curves in Germany. Here it is interesting to see if all the three available data  
 527 sets are useful for regionalisation, or if single or dual networks are enough. For this purpose, the performance  
 528 improvement exhibited by different combinations of the data types in KED (as per **Table 7**) in comparison to the  
 529 benchmark are visualised in **Figure 12**. Note that since there are 30 realisation of DS data, a boxplot is illustrating the  
 530 performance spread over these 30 realisations. This affects regionalisation methods where DS data is present, otherwise  
 531 a single line indicates the performance of the regionalisation. For very low return periods (T1a), the integration of all data  
 532 types of the form KED[LS+SS|DS] brings the best performance, with RMSE and BIAS up to 20% smaller and NSE 0.7%  
 533 higher. For return period T10a, the KED[LS|SS], KED[LS|DS] and KED[LS+SS|DS] perform very similar: some random  
 534 realisation from the disaggregated daily series (DS) introduce high improvement but as well low values, even though the  
 535 median over the 30 realisation is at the same level as the KED[LS|SS] one. For high return periods (T100a), KED[LS|SS]  
 536 introduces the highest improvement in all three performance criteria. Actually KED[LS|DS] is the second-best option,  
 537 however the median over the 30 realisations is either lower or equal to the performance of the KED[LS|SS]. There are  
 538 few realisations that introduce the highest improvements for RMSE and BIAS, nevertheless the computation time for the  
 539 disaggregation scheme and the fitting of the Koutsoyiannis approach is also a disadvantage of using the DS dataset. So  
 540 finally, the kriging interpolation of the long network (LS) with the short network (SS) as an external drift, is chosen as an

541 optimal method for the regionalisation of the GEV and Koutsoyiannis parameters. **Table 11** indicates the median  
 542 performance criteria (RMSE, PBIAS, NSE) for different return periods reached by this method (KED[LS|SS]). Expected  
 543 deterioration in performance when the long series are not present in comparison to the best method selected for  
 544 regionalisation (KED[LS|SS]) are given in **Figure A5** in the appendix.

545 **Table 11** Median cross-validation performance over 133 long series (LS) stations for the final selected regionalisation  
 546 method (KED[LS|SS]) at different return periods  $T_a$ .

	T1a	T10a	T20a	T50a	T100a
	KED[LS SS]				
<b>RMSE (%)</b>	8.11	8.06	8.24	8.46	8.86
<b>PBIAS (%)</b>	1.00	1.10	0.80	1.00	0.80
<b>NSE (-)</b>	0.982	0.981	0.979	0.979	0.980

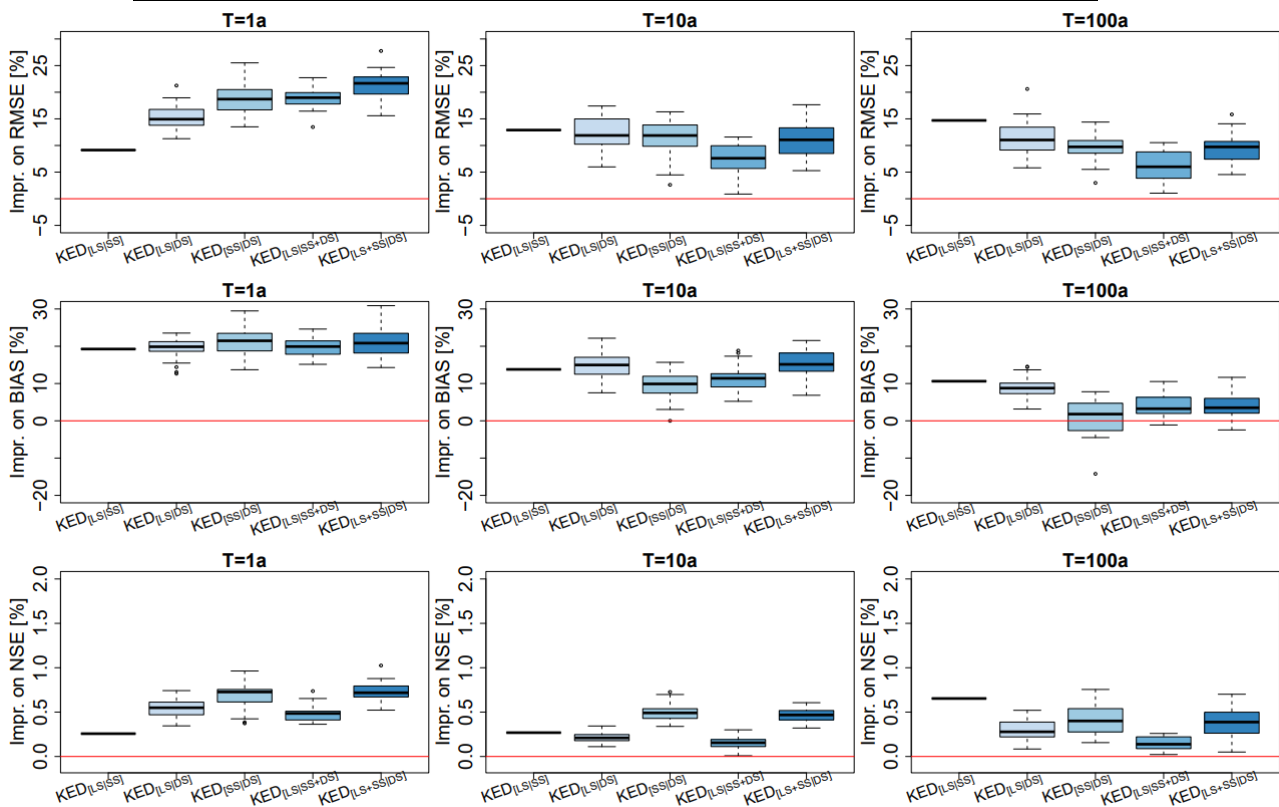


**Figure 12** Median performance improvements towards the benchmark from regionalising on different data combinations, as per **Table 7**, in kriging with external drift; where SS are short series, LS long series (LS) and DS disaggregated daily series, combined either with same importance (+) or with priority importance (/).

547 The three different data sets implemented here, distinguish from one another based on the parameter values (as shown in  
 548 **Figure A3** of the appendix) also on the spatial dependency, variograms, shown in **Figure 8**. When fixing the shape  
 549 parameter to 0.1, the location and Koutsoyiannis parameters of LS and SS, are in similar range, and the main difference  
 550 is seen at the scale parameter (where the SS has high values of the scale parameter than LS). This gives a tendency of the  
 551 short durations to estimate bigger rainfall volumes for higher return periods. This behaviour is also in agreement reported  
 552 by Madsen et al. (2017) which used a Generalised Pareto distribution also with a fix shape parameter. Typically, this is  
 553 treated by index-based regionalisation, where extremes within a region are pooled together to estimate the DDF curves at  
 554 an unknown location as done in Requena et al. (2019). However, we show here that integrating the LS and SS with  
 555 external drift kriging, hence accounting for the spatial dependency of the extremes, delivers better performance than  
 556 grouping them together in the index-based regionalisation (also valid for the LS and DS integration).



557 **4.3 Final Product and Discussion**

558 The obtained maps, on a 5km raster, for the four regionalised parameters (location parameter –  $\mu$ , scale parameter  $\sigma$ ,  
 559 Koutsoyiannis  $\theta$  and  $\eta$  parameters) with the KED[LS|SS] approach, are illustrated in **Figure 13**. Here the shape parameter  
 560 is fixed to 0.1 for whole Germany, which is very similar to results obtained by Ulrich et al. (2021) (shape parameter as  
 561 0.11 from the annual GEV approach) and validates our approach. The spatial distribution of the location GEV parameter  
 562 ( $\mu$ ) follows partly the elevation information, with higher values in the southeast, where the German Alps are located. The  
 563 scale GEV parameter ( $\sigma$ ) values are independent of the elevation, with a high localised value near to Münster city. In  
 564 2014, there was a very extreme event in Münster which has affected the statistics of the station located in the vicinity.  
 565 Currently it is not clear how to handle these singular extraordinary events in extreme value analysis in an optimal way.  
 566 Both Koutsoyiannis parameters ( $\theta$  and  $\eta$ ) show similar spatial patterns with lower values in the Alp and other mountainous  
 567 regions, as well as on the northern-west coast. These parameters exhibit higher variability in space than the GEV location  
 568 or scale parameters. Overall, the spatial distribution of  $\eta$  parameter follows the spatial structure of the annual rainfall sum  
 569 in Germany, the distribution of the location ( $\mu$ ) parameter follows the information from the elevation, while the scale ( $\sigma$ )

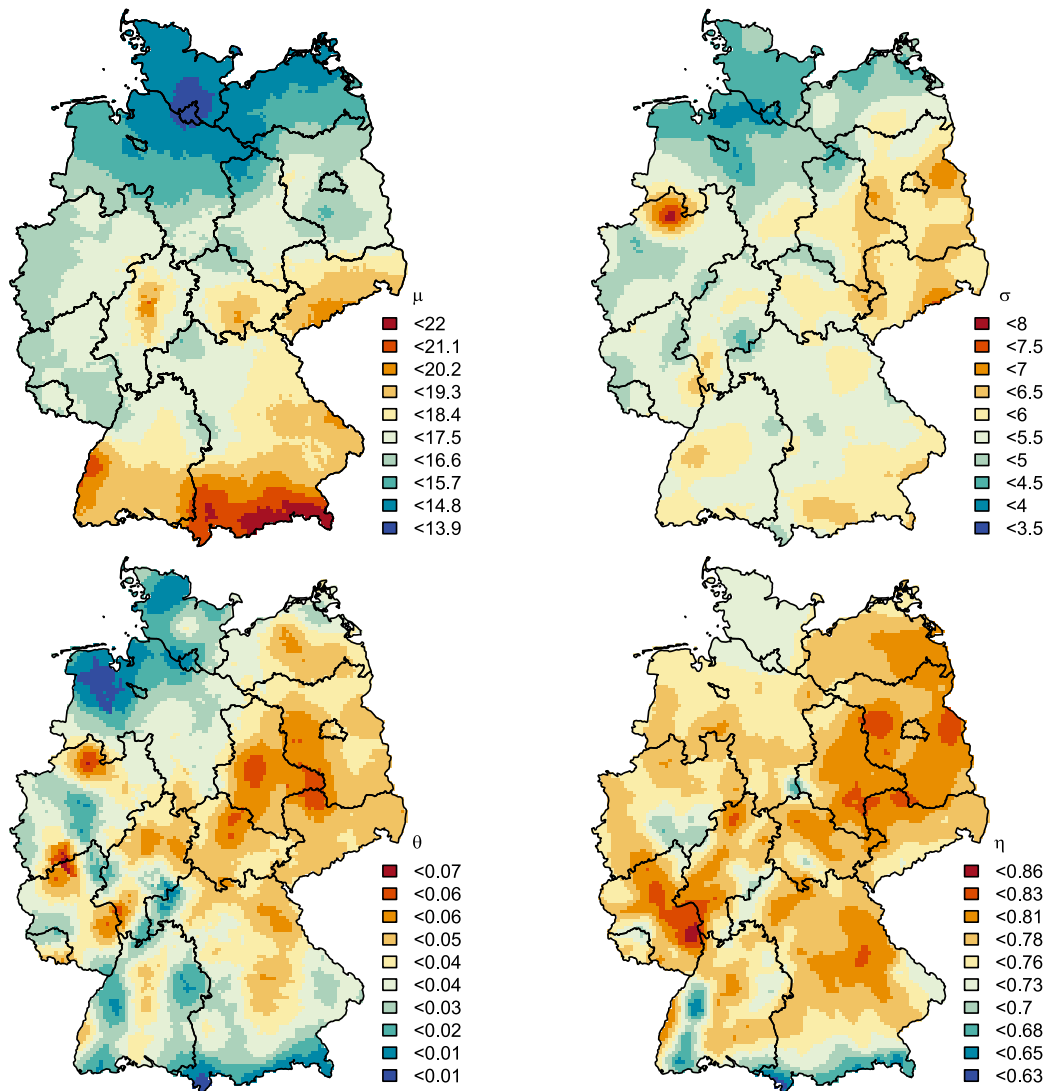
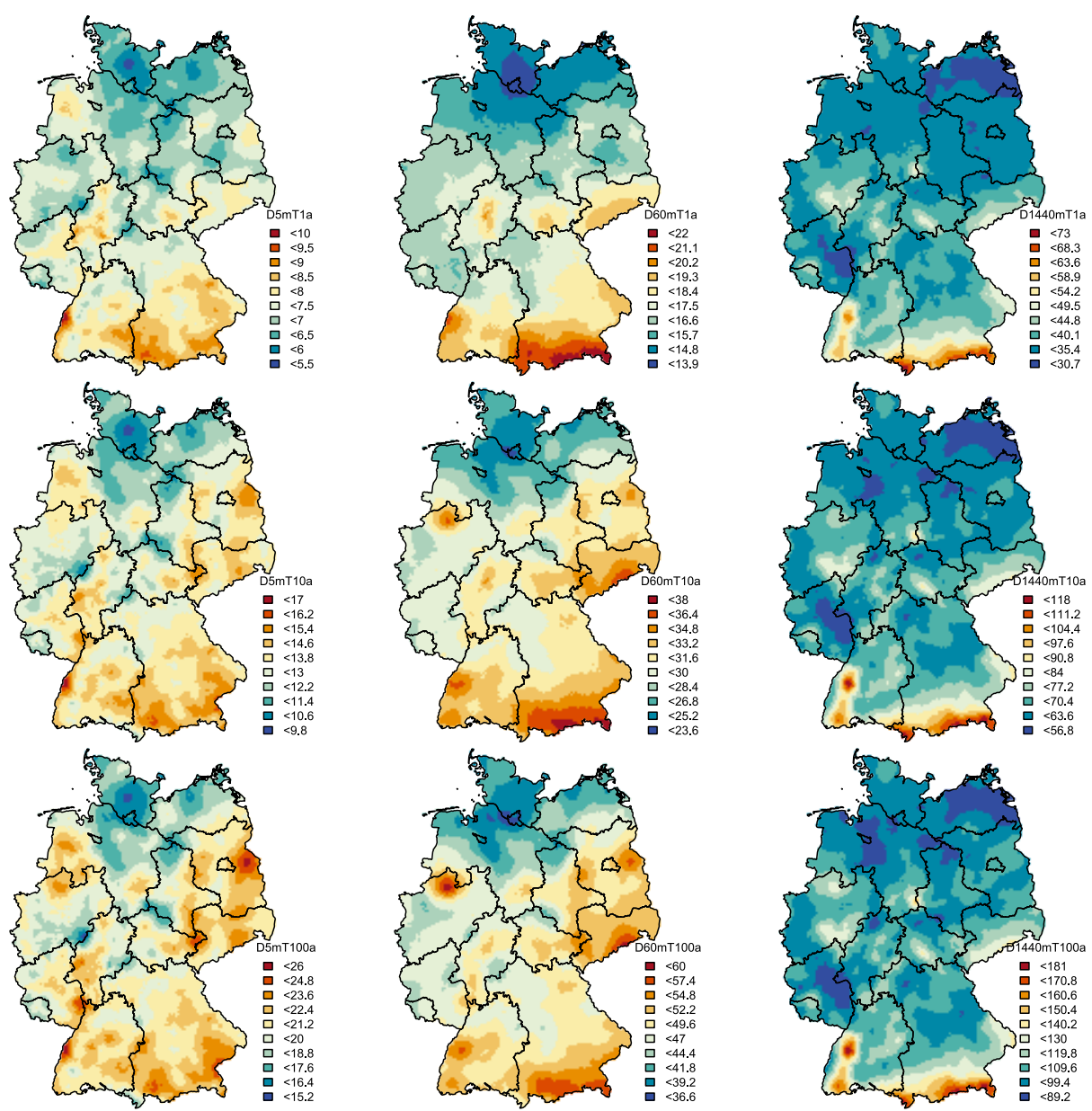


**Figure 13** Obtained interpolated maps from the KED[LS|SS] for each of the parameter: location parameter -  $\mu$ , scale parameter -  $\sigma$ , Koutsoyiannis  $\theta$  and  $\eta$  parameters. The shape parameter  $\gamma$  is kept constant at 0.1. The black lines illustrate the borders of German Federal States.

570 and  $\theta$  parameter don't seem to be influenced by any climatologic or site characteristic. This is also seen at Van De Vyver  
 571 (2012), where annual rainfall and elevation is concluded as important covariates, mainly for the location ( $\mu$ ) parameter,  
 572 while the scale ( $\sigma$ ) parameter didn't have meaningful covariates and the shape parameter didn't show any spatial structure  
 573 but was kept constant over Belgium. These results agree to a certain extend with the results obtained here. However, the  
 574 rainfall statistics extracted from short or daily series are considered as more important than the annual rainfall (which  
 575 itself is an interpolation from point observation). Thus, interpolation of long datasets, should include extreme statistics  
 576 from short or daily series rather than annual rainfall as an additional information.



577 **Figure 14** Obtained design rainfall [mm] maps for whole Germany from the KED[LS/SS] regionalisation approach  
 derived for different durations (D=5min, 60min and 1440min): first row – return period  $T_a=1$ -year, second row – return  
 period  $T_a=10$  years and third row – return period  $T_a=100$  years. The black lines illustrate the borders of German Federal  
 States.

578 With these 4 interpolated maps, together with the shape parameter fixed at 0.1, DDF curves can be obtained for any  
 579 location in Germany. Few examples of design rainfall maps for duration levels 5min, 1 hour and 1 day, and return period  
 580  $T_a=1,10,100$  years, are given in Error! Reference source not found.. For short durations (i.e. D=5 min) the spatial

581 distribution of rainfall extremes is independent from the elevation and becomes more erratic with higher return periods.  
582 This is in accordance with the fact that the convective extreme events can happen anywhere and are very low correlated  
583 with the orography. With increasing duration level, the relationship between orography and extreme rainfall becomes  
584 stronger. As for instance in  $D=1h$ , the influence of the alpine regions is visible, which becomes even stronger for the  
585 duration of  $D=1d$ . In the existing KOSTRA maps, all durations are dependent on elevation. Here, the elevation itself  
586 didn't show much effect on the scale ( $\sigma$ ) and  $\theta$  parameter, only to some extent on the location ( $\mu$ ) and  $\eta$  parameter. This  
587 means that the extremes of longer duration (affected by the  $\eta$  parameter) and of low return period (affected by the location  
588 parameter) will show a pattern resembling the elevation. This is not true for short durations (affected by the  $\theta$  parameter)  
589 and high return periods (affected by the scale parameter). This as well agrees with other studies, that report a weak  
590 dependence of short duration rainfall (shorter than 1 or 2 hours) with the elevation in Germany (Lengfeld et al., 2019).  
591 Lastly, the kriging interpolation as implemented here, opens the possibility to capture better the uncertainty – not only  
592 the sample uncertainty, which is typically done by bootstrapping the points statistics, but accounting as well the spatial  
593 structure of extremes by considering spatial simulations. Following this study and the best chosen method here, an  
594 extensive uncertainty analysis is given at (Shehu and Haberlandt, 2022), whose result propose that DDF estimates with  
595 KED[LS|SS] are more precise near to the location of long series (LS), and less precise in regions far from long series  
596 (LS).

## 597 **5. Conclusions**

598 In this study the use of three ground measuring types in Germany was investigated for the estimation of design rainfall  
599 maps. These data types included the long high-resolution dataset, with long observations at 5 min time steps from 60-70  
600 years, the short high-resolution dataset with short observation also at 5 min time steps from 10 to 20 years, and the daily  
601 dataset with observations varying from 20 to 100 years. The purpose of the work was to review different methods for the  
602 estimation and regionalisation of the DDF curves and to investigate the value and the best integration of different data  
603 types for estimating DDF curves in unobserved locations. The results will provide the basis for a new update of the design  
604 storm maps for Germany, the KOSTRA-DWD2023. First, the long analogous and recent digital high-resolution networks  
605 were homogenised by performing a jump correction, with the jumps coinciding with sensor type changes. Second the  
606 daily dataset was disaggregated to sub hourly durations based on a cascade model parameterised according to Olsson,  
607 (1998) and Lisniak et al. (2013) from the RADOLAN data in Germany. Third, Annual Maximum Series (AMS) were  
608 derived for each station available in the three datasets for duration levels ranging from 5 min to 7 days. This represents the  
609 main database for the present investigation. Two methods were investigated for local estimation of rainfall extreme  
610 statistics, adopted from Koutsoyiannis et al. (1998), and Fischer and Schumann (2018), and three different regionalisation  
611 approaches (ordinary kriging, external drift kriging and index-based regionalisation) were investigated for the spatial  
612 estimation of DDF curves in Germany. The conclusions derived, by considering the long high-resolution dataset as the  
613 truth, are summarised as:

- 614 • Both methods for local estimation of the rainfall extreme statistics behave quite similarly in capturing the  
615 local duration specific rainfall depths. Nevertheless, the estimation of parameters through the  
616 Koutsoyiannis approach is more robust in terms of data sampling uncertainties. Particularly the  
617 Koutsoyiannis approach combined with a Generalised Extreme Value (GEV) distribution with a fixed  
618 shape parameter value at 0.1 exhibited the highest robustness with tolerable decline in precision.  
619 Therefore, 4 parameters were used to describe the local statistics of extreme rainfall: the location and  
620 scale GEV parameters and the two Koutsoyiannis parameters  $\theta$  and  $\eta$ . These 4 parameters represent the  
621 basis for the testing of different scenarios and regionalisation approaches.



- 622 • When only the long high-resolution dataset is present, both ordinary kriging and index-based  
623 regionalisation perform similarly, with ordinary kriging showing slightly better median performance.  
624 This result remains true as well for other data combination settings, with kriging methods exhibiting lower  
625 RMSE and NSE, but slightly higher PBIAS than the index-based regionalisation. The only case where  
626 the index-based regionalisation has superiority against kriging, is when only short high-resolution series  
627 are present.
- 628 • When more than two datatypes are available, kriging with external drift seems more adequate for the  
629 parameter interpolation than ordinary kriging, at least regarding the RMSE and NSE performance.
- 630 • A combination of long and short high-resolution series improves the performance of regionalisation  
631 considerably (up to 15% for  $T_a=100$  years), but only when the data sets are combined with external drift  
632 kriging. Here the parameters from the short series are first interpolated with ordinary kriging, which later  
633 on, serve as an external drift for the kriging interpolation of the parameters from the long series. This  
634 combination gave overall the best results at least for return periods higher than 10 years.
- 635 • A combination of the long high-resolution and daily dataset improves the performance of regionalisation  
636 up to 10% being the second-best method for regionalisation. Here as well the best regionalisation was the  
637 external drift kriging, with the ordinary kriging interpolation of daily parameters serving as an external  
638 drift.
- 639 • A combination of the three data types improves the regionalisation considerably (up to 20%) only for low  
640 return periods (shorter or equal than 10 years).
- 641 • Overall, the best method for the regionalisation of the DDF curves in Germany, was the kriging  
642 interpolation of the long sub hourly stations, with the short sub hourly stations as an external drift. On  
643 average, this approach exhibited 8-9% RMSE (increasing with the return period) and up to 1% BIAS  
644 (decreasing with the return period) when compared to the locally estimated DDF curves.

645 The cross-validation implemented here can only describe the accuracy of the regionalisation methods when compared to  
646 the local estimation, but it does not say much about the precision of the predictions. Thus, it is important to perform an  
647 uncertainty analysis, which should include not only the local estimation of sample statistics (briefly discussed here) but  
648 as well the spatial uncertainty of the kriging interpolation. The integration of spatial uncertainty in the DDF design storms  
649 of Germany is investigated and discussed in Shehu and Haberlandt (2022). Further improvements of the methodology  
650 might include the validation of the methods on distinguished region. It has to be noted that the majority of the reference  
651 stations in Germany are located in the lowlands, thus the mountainous areas may be under-represented. It would be  
652 interesting to investigate if daily data or other site characteristics (like the elevation) are improving the performance of  
653 the chosen method in these regions. However, should one decide to perform region specific regionalisation, special care  
654 should be paid to the continuity of DDF values at the borders of the regions. Lastly, these conclusions are valid mainly  
655 for Germany, where dense networks are present. The advantage of each data set or approach may still change depending  
656 on the station density or study area location.

## 657 **6. Data Availability**

658 The daily and the short sub-daily network, as well as the other meteorological variables, are made publicly available by  
659 the German Weather Service (DWD) and can be accessed at [https://opendata.dwd.de/climate\\_environment/CDC/](https://opendata.dwd.de/climate_environment/CDC/). The

660 long sub-daily network has been digitalised and provided by the DWD. All R-codes can be provided by the corresponding  
661 authors upon request.

## 662 **7. Authors Contribution**

663 Supervision and funding for this research were acquired by UH and WW, the study conception, design and methodology  
664 were performed by all authors, while the software, data collection, derivation and interpretation of results were handled  
665 mainly by BS and WW (with support of the other authors). BS prepared the original draft, which is revised by all authors.

## 666 **8. Competing Interest**

667 The authors declare that they have no conflict of interest.

## 668 **9. Funding**

669 This research was funded by the German Ministry of Agriculture and Environment Mecklenburg-Vorpommern and the  
670 Federal State Funding Programme "Water, Soil and Waste".

## 671 **10. Acknowledgements**

672 The results presented in this study are part of the research project "Investigating Different Methods for Revising and  
673 Updating the Heavy Rainfall Statistics in Germany (MUNSTAR)", funded by the German Ministry of Agriculture and  
674 Environment Mecklenburg-Vorpommern and the Federal State Funding Programme "Water, Soil and Waste" who are  
675 gratefully acknowledged. We are also thankful for the provision and right to use the data from the German National  
676 Weather Service (Deutscher Wetterdienst DWD), more specific Thomas Deutschländer and Thomas Junghänel.

## 677 **11. References**

- 678 Asquith, W. H.: Lmomco: L-moments, censored L-moments, trimmed L-moments, L-comoments, and many  
679 distributions., 2021.
- 680 Bara, M., Kohnová, S., Gaál, L., Szolgay, J. and Hlavčová, K.: Estimation of IDF curves of extreme rainfall by simple  
681 Scaling in Slovakia, *Contrib. to Geophys. Geod.*, 39(3), 2009.
- 682 Bárdossy, A. and Pegram, G.: Combination of radar and daily precipitation data to estimate meaningful sub-daily point  
683 precipitation extremes, *J. Hydrol.*, 544, 397–406, doi:10.1016/j.jhydrol.2016.11.039, 2017.
- 684 Bartels, H., Weigl, E., Reich, T., Lang, P., Wagner, A., Kohler, O., Gerlach, N. and MeteoSolutions GmbH: Projekt  
685 RADOLAN - Routineverfahren zur Online-Aneicherung der Radarniederschlagsdaten mit Hilfe von automatischen  
686 Bodenniederschlagsstationen (Ombrometer), Offenbach am Main., 2004.
- 687 Berndt, C., Rabiei, E. and Haberlandt, U.: Geostatistical merging of rain gauge and radar data for high temporal  
688 resolutions and various station density scenarios, *J. Hydrol.*, 508, 88–101, doi:10.1016/j.jhydrol.2013.10.028, 2014.
- 689 Borga, M., Vezzani, C. and Fontana, G. D.: Regional Rainfall Depth-Duration-Frequency Equations for an Alpine  
690 Region, *Nat. Hazards*, 36, 221–235, 2005.
- 691 Burn, D. H.: A framework for regional estimation of intensity-duration-frequency (IDF) curves, *Hydrol. Process.*,  
692 28(14), doi:10.1002/hyp.10231, 2014.
- 693 Cannon, A. J.: Non-crossing nonlinear regression quantiles by monotone composite quantile regression neural network,  
694 with application to rainfall extremes, *Stoch. Environ. Res. Risk Assess.*, 32(11), doi:10.1007/s00477-018-1573-6, 2018.
- 695 Ceresetti, D., Ursu, E., Carreau, J., Anquetin, S., Creutin, J. D., Gardes, L., Girard, S. and Molinié, G.: Evaluation of  
696 classical spatial-analysis schemes of extreme rainfall, *Nat. Hazards Earth Syst. Sci.*, 12(11), 3229–3240,  
697 doi:10.5194/nhess-12-3229-2012, 2012.
- 698 Coles, S.: *An Introduction to Statistical Modeling of Extreme.*, 2001.
- 699 Delrieu, G., Wijnbrans, A., Boudevillain, B., Faure, D., Bonnifait, L. and Kirstetter, P. E.: Geostatistical radar–raingauge

700 merging: A novel method for the quantification of rain estimation accuracy, *Adv. Water Resour.*, 71, 110–124,  
701 doi:10.1016/J.ADVWATRES.2014.06.005, 2014.

702 Durrans, S. R. and Kirby, J. T.: Regionalization of extreme precipitation estimates for the Alabama rainfall atlas, *J.*  
703 *Hydrol.*, 295(1–4), doi:10.1016/j.jhydrol.2004.02.021, 2004.

704 DVWK: Statistische Analyse von Hochwasserabflüssen, Merkblatt 251, Bonn, 62 S, 1999.

705 DWA: Arbeitsblatt DWA-A 531: Starkregen in Abhängigkeit von Wiederkehrzeit und Dauer, DWA Arbeitsgruppe HW  
706 1.1e, Hennef, Deutschland., 2012.

707 Fischer, S. and Schumann, A. H.: Berücksichtigung von Starkregen in der Niederschlagsstatistik, *Hydrol. und*  
708 *Wasserbewirtschaftung*, 62(4), 221–240, doi:10.5675/HyWa, 2018.

709 Forestieri, A., Lo Conti, F., Blenkinsop, S., Cannarozzo, M., Fowler, H. J. and Noto, L. V.: Regional frequency analysis  
710 of extreme rainfall in Sicily (Italy), *Int. J. Climatol.*, 38(January), e698–e716, doi:10.1002/joc.5400, 2018.

711 Goudenhoofdt, E., Delobbe, L. and Willems, P.: Regional frequency analysis of extreme rainfall in Belgium based on  
712 radar estimates, *Hydrol. Earth Syst. Sci.*, 21(10), doi:10.5194/hess-21-5385-2017, 2017.

713 Gupta, V. K. and Waymire, E.: Multiscaling properties of spatial rainfall and river flow distributions, *J. Geophys. Res.*,  
714 95(D3), 1999–2009, doi:10.1029/JD095iD03p01999, 1990.

715 Hengl, T.: Finding the right pixel size, *Comput. Geosci.*, 32(9), 1283–1298, doi:10.1016/j.cageo.2005.11.008, 2006.

716 Holešovský, J., Fusek, M., Blachut, V. and Michálek, J.: Comparison of precipitation extremes estimation using  
717 parametric and nonparametric methods, *Hydrol. Sci. J.*, 61(13), doi:10.1080/02626667.2015.1111517, 2016.

718 Hosking, J. R. M. and Wallis, J. R.: *Regional Frequency Analysis*, Cambridge University Press., 1997.

719 Hyndman, R. J. and Fan, Y.: Sample Quantiles in Statistical Packages, *Am. Stat.*, 50(4), 361–365,  
720 doi:10.1080/00031305.1996.10473566, 1996.

721 Johnson, F. and Sharma, A.: Design Rainfall, in *Handbook of Applied Hydrology*, edited by V. P. Singh, pp. 125–3 to  
722 125–13, McGraw-Hill, New York., 2017.

723 Kebaili Bargaoui, Z. and Chebbi, A.: Comparison of two kriging interpolation methods applied to spatiotemporal  
724 rainfall, *J. Hydrol.*, 365(1–2), doi:10.1016/j.jhydrol.2008.11.025, 2009.

725 Koenker, R.: Quantile Regression, , doi:10.1017/CBO9780511754098, 2005.

726 Koutsoyiannis, D.: Statistics of extremes and estimation of extreme rainfall: I. Theoretical investigation, *Hydrol. Sci. J.*,  
727 49(4), 575–590, doi:10.1623/hysj.49.4.575.54430, 2004a.

728 Koutsoyiannis, D.: Statistics of extremes and estimation of extreme rainfall: II. Empirical investigation of long rainfall  
729 records, *Hydrol. Sci. J.*, 49(4), 591–610, doi:10.1623/hysj.49.4.591.54424, 2004b.

730 Koutsoyiannis, D., Kozonis, D. and Manetas, A.: A mathematical framework for studying rainfall intensity-duration-  
731 frequency relationships, *J. Hydrol.*, 206(1–2), 118–135, doi:10.1016/S0022-1694(98)00097-3, 1998.

732 Lengfeld, K., Winterrath, T., Junghänel, T., Hafer, M. and Becker, A.: Characteristic spatial extent of hourly and daily  
733 precipitation events in Germany derived from 16 years of radar data, *Meteorol. Zeitschrift*, 28(5), 363–378,  
734 doi:10.1127/metz/2019/0964, 2019.

735 Licznar, P., De Michele, C. and Adamowski, W.: Precipitation variability within an urban monitoring network via  
736 microcanonical cascade generators, *Hydrol. Earth Syst. Sci.*, 19(1), 485–506, doi:10.5194/hess-19-485-2015, 2015.

737 Lisniak, D., Franke, J. and Bernhofer, C.: Circulation pattern based parameterization of a multiplicative random cascade  
738 for disaggregation of observed and projected daily rainfall time series, *Hydrol. Earth Syst. Sci.*, 17(7), 2487–2500,  
739 doi:10.5194/hess-17-2487-2013, 2013.

740 Madsen, H., Arnbjerg-Nielsen, K. and Mikkelsen, P. S.: Update of regional intensity-duration-frequency curves in  
741 Denmark: Tendency towards increased storm intensities, *Atmos. Res.*, 92(3), doi:10.1016/j.atmosres.2009.01.013,

742 2009.

743 Madsen, H., Gregersen, I. B., Rosbjerg, D. and Arnbjerg-Nielsen, K.: Regional frequency analysis of short duration  
744 rainfall extremes using gridded daily rainfall data as co-variate, *Water Sci. Technol.*, 75(8), doi:10.2166/wst.2017.089,  
745 2017.

746 Marra, F., Nikolopoulos, E. I., Anagnostou, E. N., Bárdossy, A. and Morin, E.: Precipitation frequency analysis from  
747 remotely sensed datasets: A focused review, *J. Hydrol.*, 574(March), 699–705, doi:10.1016/j.jhydrol.2019.04.081,  
748 2019.

749 Müller, H. and Haberlandt, U.: Temporal rainfall disaggregation using a multiplicative cascade model for spatial  
750 application in urban hydrology, *J. Hydrol.*, 556, 847–864, doi:10.1016/J.JHYDROL.2016.01.031, 2018.

751 Olsson, J.: Evaluation of a scaling cascade model for temporal rain- fall disaggregation, *Hydrol. Earth Syst. Sci.*, 2(1),  
752 19–30, doi:10.5194/hess-2-19-1998, 1998.

753 Paixao, ; E, Auld, H., Mirza, M. M. Q., Klaassen, J. and Shephard, M. W.: Regionalization of heavy rainfall to improve  
754 climatic design values for infrastructure: case study in Southern Ontario, Canada, *Hydrol. Sci. Journal-Journal des Sci.*  
755 *Hydrol.*, 56(7), 1067–1089, doi:10.1080/02626667.2011.608069, 2011.

756 Papalexiou, S. M.: Unified theory for stochastic modelling of hydroclimatic processes: Preserving marginal  
757 distributions, correlation structures, and intermittency, *Adv. Water Resour.*, 115, doi:10.1016/j.advwatres.2018.02.013,  
758 2018.

759 Papalexiou, S. M. and Koutsoyiannis, D.: Battle of extreme value distributions : A global survey on extreme daily  
760 rainfall, *Water Resour. Res.*, 49(1), 187–201, doi:10.1029/2012WR012557, 2013.

761 Pebesma, E. J.: Multivariable geostatistics in S: The gstat package, *Comput. Geosci.*, 30(7), 683–691,  
762 doi:10.1016/j.cageo.2004.03.012, 2004.

763 Requena, A. I., Burn, D. H. and Coulibaly, P.: Pooled frequency analysis for intensity–duration–frequency curve  
764 estimation, *Hydrol. Process.*, 33(15), doi:10.1002/hyp.13456, 2019.

765 De Salas, L. and Fernández, J. A.: “In-site” regionalization to estimate an intensity-duration-frequency law: a solution  
766 to scarce spatial data in Spain, *Hydrol. Process. Hydrol. Process*, 21, 3507–3513, doi:10.1002/hyp.6551, 2007.

767 Shehu, B. and Haberlandt, U.: Uncertainty estimation of regionalised depth-duration-frequency curves in Germany,  
768 *Hydrol. Earth Syst. Sci.*, [preprint], in review, doi:https://doi.org/10.5194/hess-2022-254, 2022.

769 Smithers, J. C. and Schulze, R. E.: A methodology for the estimation of short duration design storms in South Africa  
770 using a regional approach based on L-moments, *J. Hydrol.*, 241(1–2), doi:10.1016/S0022-1694(00)00374-7, 2001.

771 Uboldi, F., Sulis, A. N., Lussana, C., Cislighi, M. and Russo, M.: A spatial bootstrap technique for parameter  
772 estimation of rainfall annual maxima distribution, *Hydrol. Earth Syst. Sci.*, 18(3), 981–995, doi:10.5194/hess-18-981-  
773 2014, 2014.

774 Ulrich, J., Jurado, O. E., Peter, M., Scheibel, M. and Rust, H. W.: Estimating idf curves consistently over durations with  
775 spatial covariates, *Water (Switzerland)*, 12(11), 1–22, doi:10.3390/w12113119, 2020.

776 Ulrich, J., Fauer, F. S. and Rust, H. W.: Modeling seasonal variations of extreme rainfall on different timescales in  
777 Germany, *Hydrol. Earth Syst. Sci.*, 25(12), doi:10.5194/hess-25-6133-2021, 2021.

778 Viglione, A., Hosking, J. R. M., Laio, F., Miller, A., Gaume, E., Payrastre, O., Salinas, J. L., N’guyen, C. C. and  
779 Halbert, K.: Non-Supervised Regional Flood Frequency Analysis., 2020.

780 Van de Vyver, H.: Bayesian estimation of rainfall intensity-duration-frequency relationships, *J. Hydrol.*, 529,  
781 doi:10.1016/j.jhydrol.2015.08.036, 2015.

782 Van De Vyver, H.: Spatial regression models for extreme precipitation in Belgium, *Water Resour. Res.*, 48(9), 1–17,  
783 doi:10.1029/2011WR011707, 2012.

784 Ward, J. H.: Hierarchical Grouping to Optimize an Objective Function, *J. Am. Stat. Assoc.*, 58(301), 236–244,  
785 doi:10.1080/01621459.1963.10500845, 1963.  
786 Watkins, D. W., Link, G. A. and Johnson, D.: Mapping regional precipitation intensity duration frequency estimates, *J.*  
787 *Am. Water Resour. Assoc.*, 41(1), doi:10.1111/j.1752-1688.2005.tb03725.x, 2005.  
788

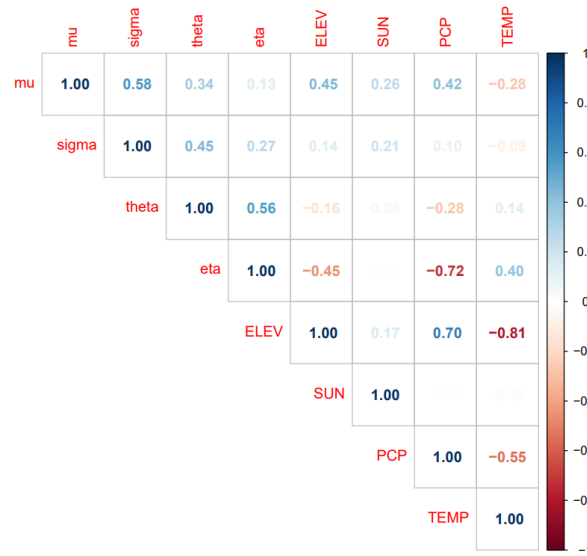


**Figure A1** Cross-correlation between the selected local parameters (Koutsoyiannis and GEV parameters) for regionalisation and useful site characteristics that might act as an external drift information. Mu is the GEV location parameter, sigma the GEV scale parameter, theta and eta the Koutsoyiannis parameters, ELEV is short for elevation information, SUN is short for long term average of annual sunshine duration, PCP is short for long term average of annual rainfall amount, and TEMP is short for the long-term average of annual mean temperature.

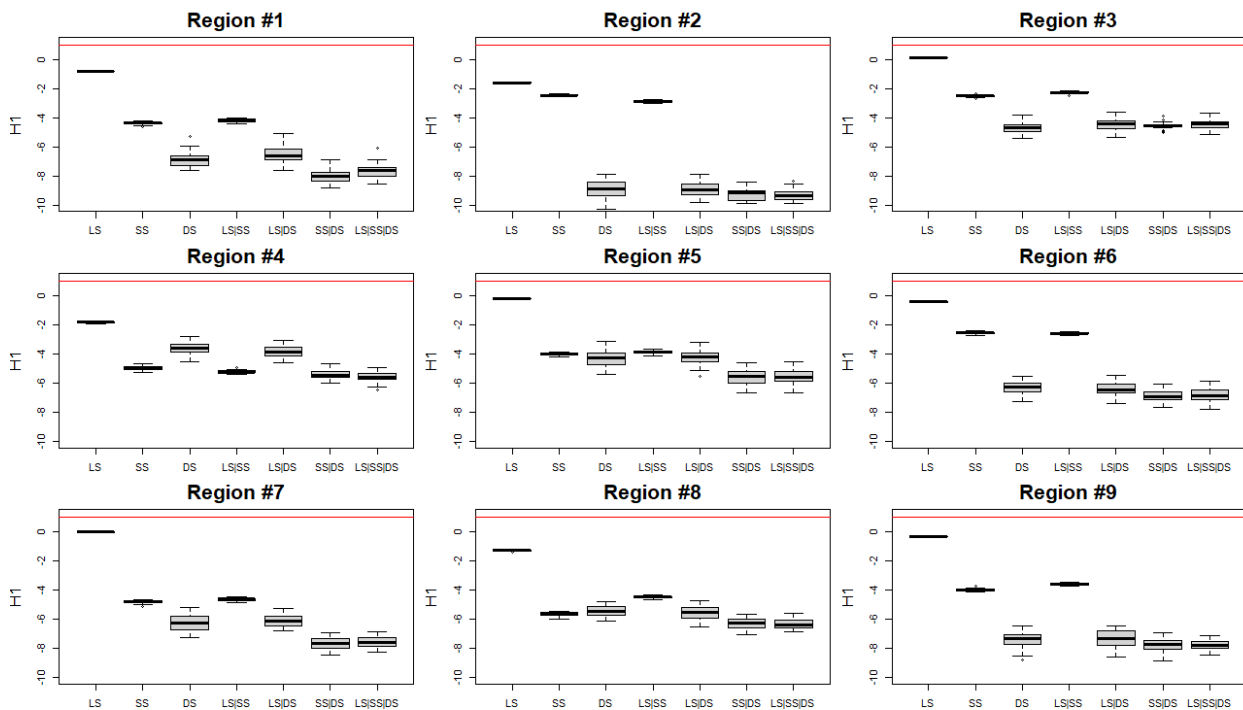


**Figure A2** The homogeneity index ( $H_1$ ) computed for each of the 9th selected regions for each of the dataset combinations.

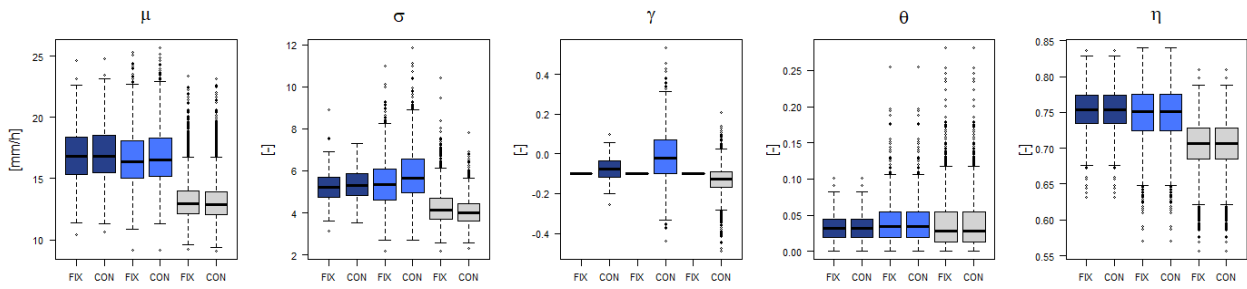


**Figure A3** Koutsoyiannis parameters obtained for each data set (LS in dark blue, SS in light blue and DS in grey) when fixing the shape parameter to 0.1 for all stations (FIX) or constant over all durations per each station (CON).

793

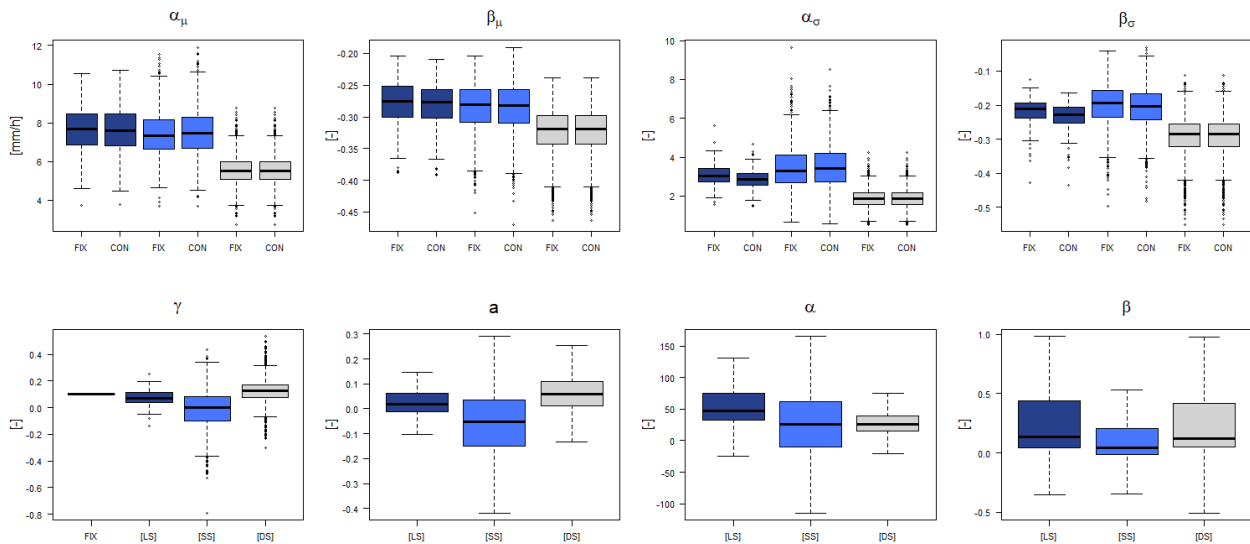


**Figure A4** Fischer/Schumann parameters obtained for each data set (LS in dark blue, SS in light blue and DS in grey) when fixing the shape parameter to 0.1 (FIX) or constant over all durations per each station (CON).

794

	RMSE (%)					PBIAS (%)					NSE (%)				
	T1a	T10a	T20a	T50a	T100a	T1a	T10a	T20a	T50a	T100a	T1a	T10a	T20a	T50a	T100a
SS	8.5	0.4	0.5	-8.1	-12.0	0.3	8.1	5.1	-1.2	-6.1	0.1	0.4	-0.3	-0.3	-0.6
DS	-53.1	-42.2	-40.9	-36.4	-34.3	-59.3	-35.7	-26.6	-25.8	-21.2	-2.6	-1.8	-1.8	-1.8	-1.8
SS + DS	9.6	-1.0	-0.6	-3.3	-5.0	2.2	-3.9	-1.6	-5.6	-8.8	0.5	0.2	-0.1	-0.1	-0.3

**Figure A5** Obtained Deterioration (-) or Improvement (+) towards the best regionalisation technique (KED[LS/SS]) when no long series are available (LS) and the regionalisation is performed based on short series (SS), disaggregated daily series (DS), or on both SS and DS.

795